https://doi.org/10.5194/egusphere-2026-6672
Preprint. Discussion started: 25 November 2026
© Author(s) 2026. CC BY 4.0 License.

Coupling modeled colluvium depth, landslide initiation, and debris-flow runout to map regional-scale inundation susceptibility

Nicolas W. Mathews[1], Joshua J. Roering[2], Adelaide C. Johnson[3], Luka Silva[1], Stephen McKay[4], Lauren E. Bell[1]

[1]Sitka Sound Science Center, Sitka, AK, 99835, USA
[2]Department of Geology, University of Oregon, Eugene, OR, 97403, USA
[3]Community Collaborators Organization, Juneau, AK, USA
[4]USDA Forest Service, Tongass National Forest

Correspondence to: Nicolas W. Mathews (nmathews@sitkascience.org)

Abstract

In post-glacial mountain landscapes, shallow landslides can transition into debris flows that threaten communities and infrastructure. Landslide susceptibility maps are important for identifying where landslides may occur and mitigating landslide risk, but regional-scale models often rely on first-order terrain metrics, such as slope and relief, and may not resolve local topographic controls on landslide initiation. Furthermore, landslide susceptibility models are rarely coupled with runout models to identify potential downslope inundation. Here, we coupled a physics-based landslide initiation model with a regional-scale runout model to estimate potential debris flow inundation across a large swath of Prince of Wales Island, Alaska. Using a high-resolution digital terrain model, the initiation model estimated groundwater conditions from topographic wetness and simulated spatially variable colluvium depth using models for soil production and transport. Compared with a landslide inventory, the initiation model exhibited strong discriminatory skill between inventoried initiation points and non-landslide terrain (AUC = 0.86), highlighting how spatially variable colluvium and groundwater conditions can distinguish potentially unstable convergent terrain from surrounding steep terrain. We calibrated debris-flow entrainment parameters independently within HUC-14 watersheds by optimizing agreement between modeled and inventoried landslides, capturing spatial variability in debris-flow mobility across the study area. Our results also indicate that modeled colluvium depth can be used to inform sediment availability for debris-flow entrainment, extending the utility of modeled colluvium beyond landslide initiation. The resulting debris-flow susceptibility maps estimate potential inundation at spatial scales relevant to assessing the exposure of roads, infrastructure, and communities to landslide hazards. These maps were developed through iterative collaboration with Tribal governments and community partners to link regional landslide modeling to locally relevant risk-reduction needs.

https://doi.org/10.5194/egusphere-2026-6672
Preprint. Discussion started: 25 November 2026
© Author(s) 2026. CC BY 4.0 License.

1 Introduction

Post-glacial mountain landscapes are shaped by shallow landslides, which redistribute soil and sediment (Swanston, 1969), cycle nutrients (Walker and Shiels, 2012), and sustain aquatic habitats (Geertsema and Pojar, 2007). Shallow landslides commonly initiate in steep areas of hillslope convergence, where colluvium and groundwater concentrate to reduce slope stability (Dietrich et al., 1995, 2020; Montgomery and Dietrich, 1994). The spatial distribution of colluvium depth is an important control on where slope failures can occur, while transient hydrological conditions control when slopes reach failure (Baum et al., 2010; Iverson, 2000). Because these process controls are challenging to represent across landscapes, landslide susceptibility models commonly rely on first-order metrics derived from topography, such as slope and relief (e.g., Mirus et al., 2024). Although sufficient colluvium depth is a precursor for shallow landslide occurrence (Parker et al., 2016), its spatial variability is only sometimes incorporated in landslide susceptibility models (Catani et al., 2010; Dietrich et al., 1995; Mathews et al., 2024; Pollock and Wartman, 2026; Prancevic et al., 2020), and when it is, it is often computed using empirical relationships based on curvature (Catani et al., 2010; Patton et al., 2018) that may overestimate colluvium in steep channels where transport outpaces soil production (Heimsath et al., 2012).

Landslides can pose significant risks to downslope communities and the natural environment (Schuster and Highland, 2007). Reducing these risks relies largely on improving situational awareness by identifying where and when landslides are likely to occur (Corominas et al., 2013). Landslide susceptibility maps are widely used to support hazard mitigation by identifying where future slope failure is likely (Highland and Bobrowsky, 2008). Probabilistic methods of determining landslide susceptibility rely on statistical relationships between physical attributes and known landslides to define the likelihood of landslide initiation (Reichenbach et al., 2018). These approaches are efficient, which makes their application to broad landscapes attractive, and can incorporate terrain metrics such as slope, curvature, and convergence to capture landslide probability. However, probabilistic methods account for physical controls indirectly and generally do not estimate characteristics such as landslide volume that are useful for subsequent debris-flow modeling. Alternatively, physics-based approaches simulate physical processes that contribute to landslide initiation and can estimate failure location, timing, and volume. For example, infinite-slope stability models coupled with topographic models of groundwater convergence have been used to predict shallow landslide initiation based on slope and contributing area (Montgomery and Dietrich, 1994; Pack et al., 1998), while transient models such as TRIGRS incorporate rainfall infiltration and changes in pore pressure through time (Baum et al., 2010; Godt et al., 2006). A primary challenge with physics-based approaches is constraining spatially and temporally variable parameters, such as hydrological conditions, shear strength, and colluvium depth. Colluvium depth, including unconsolidated soil and rock fragments, is often treated as spatially uniform despite evidence that its spatial distribution, which preconditions hillslopes for failure, can be estimated using long-term soil production and downslope transport (Dietrich et al., 1995; Heimsath et al., 1999; Roering, 2008). Landscape-evolution models can capture this process explicitly, translating long-term hillslope processes into spatially variable estimates of colluvium depth. This enables the

https://doi.org/10.5194/egusphere-2026-6672
Preprint. Discussion started: 25 November 2026
© Author(s) 2026. CC BY 4.0 License.

identification of localized, failure-prone portions of steep hillslopes (i.e., colluvial hollows) while also informing the volume of individual potential failures (Bellugi et al., 2015; Mathews et al., 2024; Milledge et al., 2014).

In many steep landscapes, the consequences of shallow landsliding are governed not only by where landslides initiate, but also by their transition into higher-mobility debris flows capable of inundating areas well beyond the landslide source (Hungr et al., 2014; Iverson, 1997). Inundation is typically simulated using runout models ranging from empirical approaches that relate inundation area to debris-flow volume and route material across topography (e.g, LAHARZ, Iverson et al., 1998; Griswold & Iverson, 2008; DFLOWZ, Berti & Simoni, 2007; Flow-R, Horton et al., 2013; ProDF, Gorr et al., 2022; Grfin Tools, Reid et al., 2025; Brien et al., 2025; Reid et al., 2026) or physics-based approaches that simulate processes such as momentum, particle-fluid interactions, and rheology (e.g., DAN, Hungr, 1995; DAN3D, McDougall & Hungr, 2004; RAMMS, Christen et al., 2010; D-Claw, Iverson & George, 2014). Which model is most appropriate depends on the context of its application: empirical runout models can efficiently estimate inundation at regional scales while physics-based models represent a broader suite of physical processes but are computationally expensive and require substantial parameterization (McDougall, 2017). Empirical models that can simulate key physical processes offer a useful balance for regional-scale assessments. A key process that governs debris-flow volume and inundation is volumetric growth through the entrainment of material during transport (Berger et al., 2011; Reid et al., 2016). However, entrainment is not accounted for in many regional runout approaches, and where it is included, parameters controlling volumetric growth can be difficult to constrain across heterogeneous landscapes (McDougall, 2017).

In soil-mantled landscapes, debris flows often initiate as shallow landslides, but the physics of these processes are rarely accounted for in runout models that simulate entrainment (Keck et al., 2024), especially at the regional scale (Brien et al., 2025; Pollock and Wartman, 2026). Landslide susceptibility maps identify terrain where failure might occur but often do not characterize volumes of discrete landslides useful for simulating runout, while runout models simulate inundation but are limited in their ability to differentiate initiation potential in steep, complex terrain. Coupling these processes connects the controls that distinguish localized, failure-prone locations from surrounding, relatively stable yet steep terrain with subsequent debris-flow propagation, while also providing the initial debris-flow volume needed to simulate downstream inundation. Further, although runout is influenced by long-term soil production and erosion (Jakob et al., 2005), the spatial distribution of colluvium is rarely accounted for in regional-scale models that simulate debris-flow entrainment, especially at the regional scale. Therefore, colluvium depth is a potential link between hillslope evolution, landslide susceptibility, initial debris-flow volume, and the availability of material for subsequent debris-flow entrainment.

Southeast Alaska is a steep, post-glacial landscape where colluvium overlying glacial till and bedrock produces frequent shallow landslides that often transition into debris flows, making it an ideal setting for evaluating how colluvium depth influences landslide initiation and runout. Recent fatal landslides in Sitka, Haines, Wrangell, and Ketchikan have demonstrated the consequences of landslides to human life, while numerous other landslide events have damaged power infrastructure and critical transportation corridors throughout the region (Darrow et al., 2022; Darrow and Jacobs, 2026; Kheiry, 2019; Moran, 2026; Patton et al., 2023; Roering et al., 2025). The large geographic extent and sparse hydrologic and geotechnical

https://doi.org/10.5194/egusphere-2026-6672
Preprint. Discussion started: 25 November 2026
© Author(s) 2026. CC BY 4.0 License.

characterization of Southeast Alaska make detailed site-specific assessment impractical. However, the region has an extensive landslide inventory and widespread lidar coverage that can be leveraged to develop and test regional-scale models. This combination of widespread landslide activity, limited field observations, and regional datasets requires approaches that can represent key controls on landslide initiation and debris-flow mobility across broad landscapes while accommodating spatial variability in model parameters and data sparsity.

The goals of this study were to (1) assess whether spatially variable colluvium depth and topographically derived soil saturation better identifies shallow landslide initiation compared to uniform distributions, (2) couple modeled landslide initiation locations and volumes with a regional-scale runout model that simulates entrainment, (3) develop a calibration approach that captures the spatial heterogeneity of debris-flow mobility across a large landscape, and (4) test the use of modeled colluvium depth to inform debris-flow entrainment. To accomplish these goals, we developed a coupled framework for debris-flow susceptibility mapping that links a physics-based landslide initiation model with an empirical regional-scale debris-flow runout model, calibrated to capture spatially variable debris flow mobility throughout a large landscape. We applied this framework to develop debris-flow initiation and inundation susceptibility maps for a large region of Prince of Wales Island, Southeast Alaska, USA. Our results demonstrate that accounting for the spatial distribution of colluvium improves prediction of shallow landslide initiation while yielding initiation volumes for regional debris-flow modeling, and that catchment-scale calibration of debris-flow mobility provides a practical approach for applying runout models across large landscapes.

2 Study area: Prince of Wales Island, Alaska, USA

2.1 Climate, geology, and landscape

The study area encompasses a 1,628 km^2 east-west swath of land through central Prince of Wales Island, located within the temperate rainforest of the Alexander Archipelago in Southeast Alaska, USA (Figure 1). Prince of Wales Island is in the southern reaches of the Southeast Alaska, where exposure to North Pacific storms produce approximately 216 to 254 cm of precipitation annually, with 38 cm more annual precipitation in the west-coast community of Craig (Station ID: USC00502227) than the east-coast community of Thorne Bay (Station ID: USC00509148; Palecki et al., 2021). The majority of rainfall occurs from September to January, in large part due to atmospheric rivers which are responsible for most of the extreme rainfall events in the region (Nash et al., 2024).

The landscape is characterized by steep, forested, post-glacial mountains mantled by colluvium and weathered glacial deposits (Swanston, 1969). Where present, glacial till may be part of the failure-prone soil mantle or form a low-permeability surface upon which shallow landslides fail (Swanston, 1969). The underlying geology is composed of stratified sedimentary, intrusive, and metamorphic rocks of the Alexander terrane (Gehrels, 1990). Large-scale deglaciation occurred approximately 15 to 13 kya (Baichtal et al., 2021; Carrara et al., 2003; Menounos et al., 2017) and was followed by soil formation and the establishment of widespread, mixed conifer forests which have been partially subjected to timber harvest since the 1950s (Harris and Farr, 1974; Wu et al., 1979).

https://doi.org/10.5194/egusphere-2026-6672
Preprint. Discussion started: 25 November 2026
© Author(s) 2026. CC BY 4.0 License.

2.2 Landslide processes and inventory

Prince of Wales Island has a long history of landslide research, particularly in the Maybeso Valley northwest of Hollis (Figure 1), where early field studies established important physical controls on shallow landslides and debris flows in Southeast Alaska (Swanston, 1969, 1970). Mass wasting from shallow landslides and debris flows originating in colluvial hollows is the dominant driver of erosion in the region (Swanston, 1969; Swanston and Marion, 1991). Colluvium is generally less than 1–1.5 m thick, and surface runoff is uncommon due to a substantial surficial duff layer and rapid subsurface water transmission through macropore networks (Patric and Swanston, 1968).

In contrast to many regions where shallow landslide initiation is controlled by transient changes in soil moisture and the loss of matric suction (Baum et al., 2010; Lu and Likos, 2006), slope failure in Southeast Alaska typically occurs during fully saturated, or even artesian, groundwater conditions (Mirus et al., 2025; Patric and Swanston, 1968; Sidle, 1984). Intense rainfall delivered by atmospheric rivers is the predominant trigger of landslides in the region. Recent atmospheric rivers in 1993, 2020, 2022, and 2023 have triggered widespread landsliding on Prince of Wales and surrounding islands (Lawrence et al., 2025). The majority of landslides on Prince of Wales Island have occurred on southwest to southeast facing hillslopes, corresponding to the predominant direction of atmospheric rivers (Nash et al., 2024; Roering et al., 2026).

Landslide activity on Prince of Wales Island has been exacerbated by anthropogenic and natural disturbances. Timber harvest, yellow-cedar decline, and forest road construction can increase landslide susceptibility through hydrological disturbance and the decay of reinforcement from tree root systems (Bishop and Stevens, 1964; Buma and Johnson, 2015; Johnson and Wilcock, 2002; USDA Forest Service, 2024; Wu et al., 1979), while natural disturbances such as blowdown from strong winds have also been shown to influence shallow landslide susceptibility, generally on wind-exposed southerly aspects (Buma and Johnson, 2015). Shallow landslides often develop into debris flows whose paths typically follow channels or widen into wedge-shaped runout paths (Figure 2; Swanston, 1969). Debris flows in Southeast Alaska generally exhibit lower mobility than those in global inventories, partly because post-glacial valley morphology, characterized by abrupt transitions from steep hillslopes to broad valley floors (Johnson et al., 2000). Further, mobility in Southeast Alaska has been shown to decrease with forest stand age (Booth et al., 2020).

Historical landslides have been documented throughout Southeast Alaska by the United States Forest Service in the Tongass National Forest Landslide Inventory (TNFLI), which consists of over 14,000 landslide initiation points and polygons showing the full mapped landslide extent (U.S. Forest Service, 2024b, 2024a). More than 3,600 of these landslides occurred on Prince of Wales Island and 1,251 of these landslides exist within the study area (Figure 1). These data are used throughout this study to validate the landslide initiation model and calibrate the debris-flow runout model.

2.3 Communities and infrastructure

Communities within the study area include the cities of Craig and Klawock on the western coast of Prince of Wales Island and the communities of Hollis, Thorne Bay, and Kasaan on the eastern side of the island, in addition to numerous residents

https://doi.org/10.5194/egusphere-2026-6672
Preprint. Discussion started: 25 November 2026
© Author(s) 2026. CC BY 4.0 License.

living in smaller unincorporated communities (Figure 1). Land ownership and management are primarily divided among the Tongass National Forest, Alaska Native corporations, the State of Alaska, and private landowners. Prince of Wales Island lies within the traditional homelands of the Haida and Tlingit peoples, who have stewarded these lands since time immemorial.

Prince of Wales Island hosts the most extensive connected road network in Southeast Alaska, providing critical connections among dispersed communities and access to public services, subsistence areas, inter-island ferry transportation, and other resources. Many parts of this road network are exposed to landslide risk and have been subjected to landslides severing connectivity between remote communities (e.g., Kheiry, 2019). These impacts, as well as recent fatal landslides in the nearby communities of Sitka, Haines, Wrangell, and Ketchikan, have further increased regional interest in understanding and mitigating landslide risk. The combination of widespread landslide activity, extensive transportation infrastructure, and dispersed communities underscores the need to develop regional-scale approaches that can identify both likely landslide initiation areas and potential downstream inundation across Prince of Wales Island.

https://doi.org/10.5194/egusphere-2026-6672
Preprint. Discussion started: 25 November 2026
© Author(s) 2026. CC BY 4.0 License.

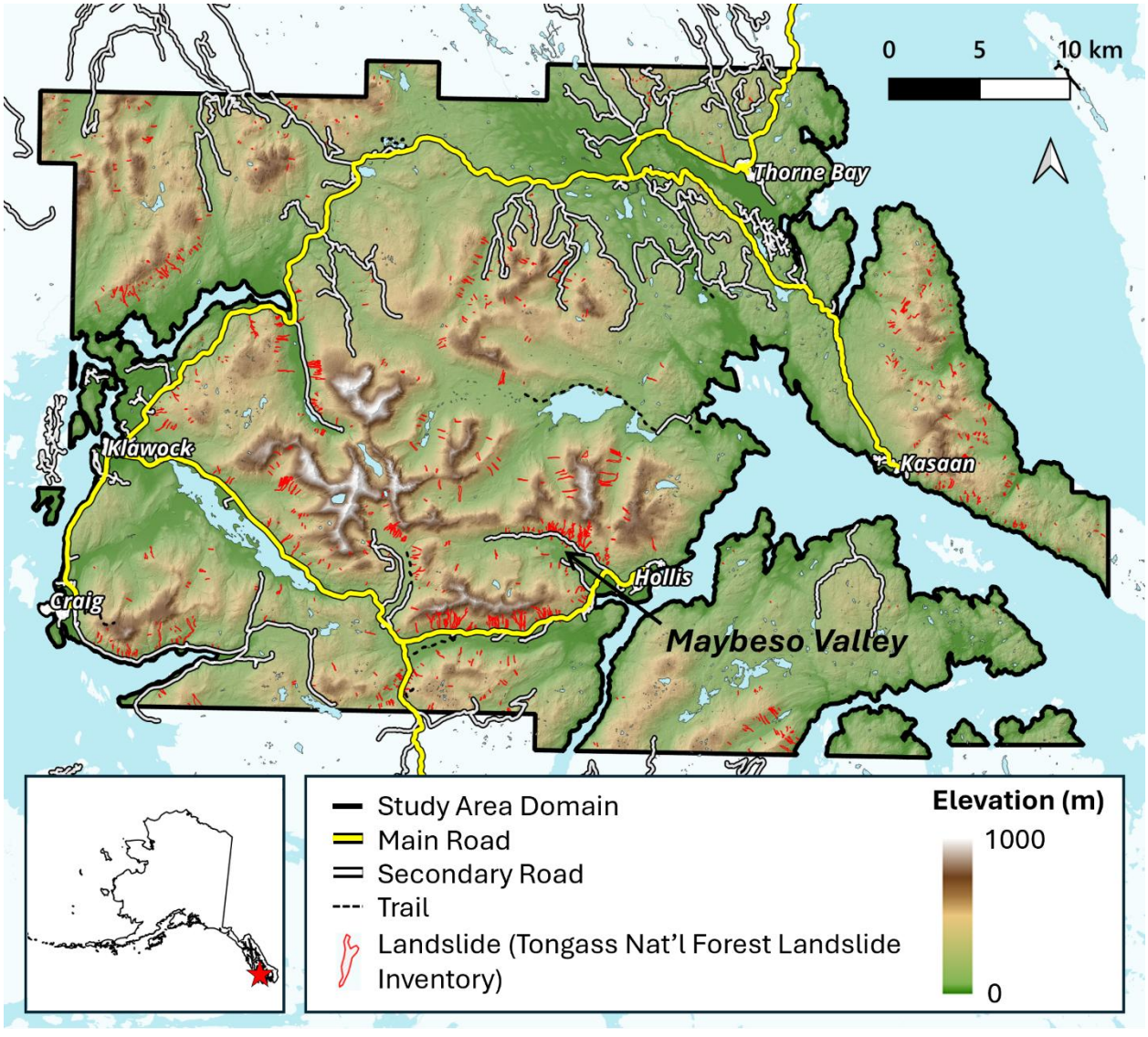

Figure 1 Map of study area on Prince of Wales Island, Southeast Alaska, USA. Elevation and hillshade derived from lidar (Quantum Spatial, 2018, 2020). Road data © OpenStreetMap contributors (openstreetmap.org/copyright). Water bodies from the SeaVoX Salt and Fresh Water Body Gazetteer (British Oceanographic Data Centre, 2023). Inset state boundary from U.S. Census Bureau (2019).

https://doi.org/10.5194/egusphere-2026-6672
Preprint. Discussion started: 25 November 2026
© Author(s) 2026. CC BY 4.0 License.

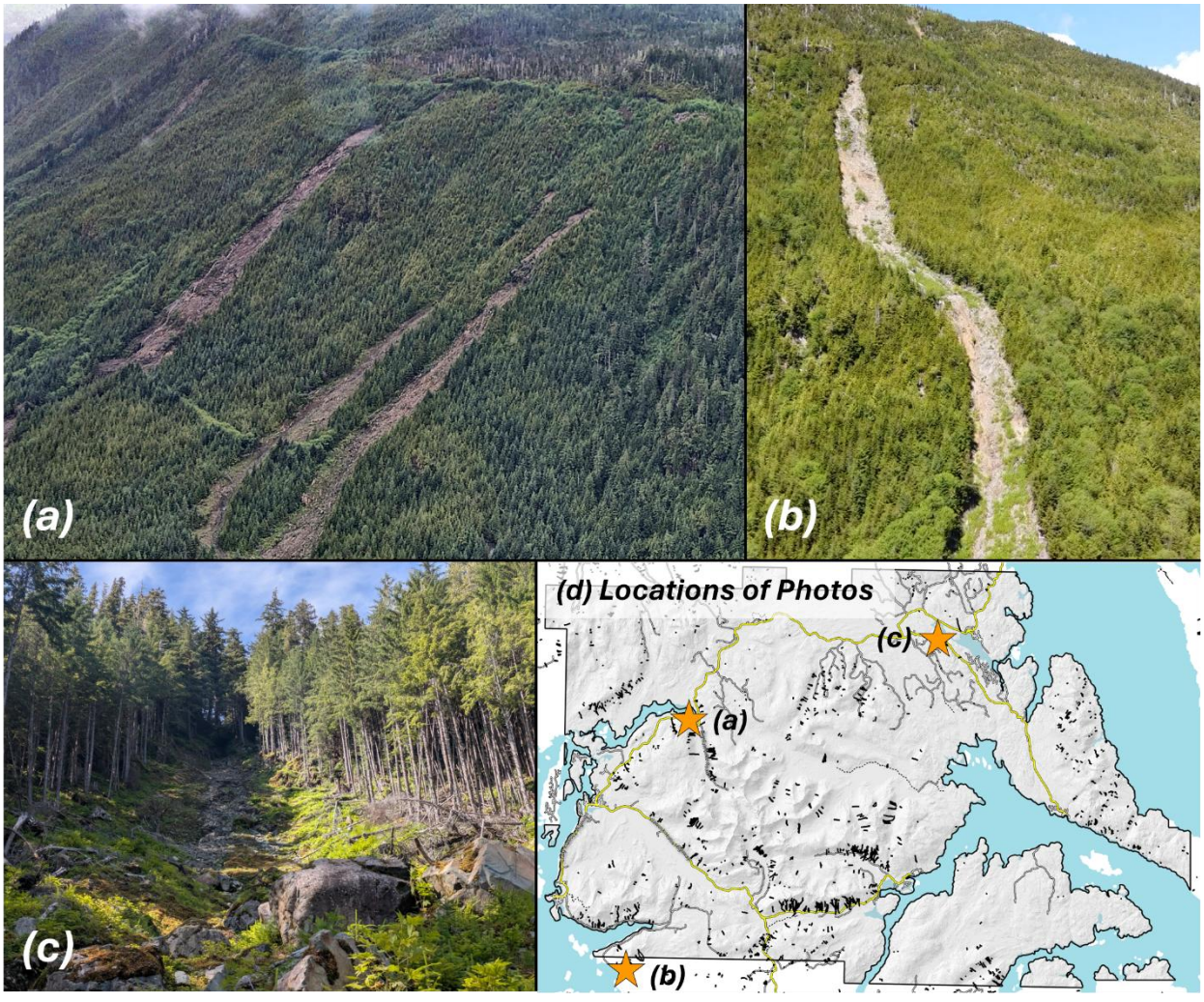

175 Figure 2 Landslides on Prince of Wales Island: (a) A series of debris flows following gently channelized topography and impacting Big Salt Road, northeast of Klawock, AK (photo: N. W. Mathews). (b) A debris flow on a southerly aspect south of Port Saint Nicholas, a bay east of Craig, AK (photo: A. Vale). (c) A wedge-shaped debris flow that blocked the road between Kasaan and Thorne Bay, AK, for several months (photo: N. W. Mathews). (d) Approximate photo locations (yellow and white lines show roads; black polygons show TNFLI landslide areas). Hillshade derived from lidar (Quantum Spatial, 2018, 2020). Road data © OpenStreetMap contributors
180 (openstreetmap.org/copyright). Water bodies from the SeaVoX Salt and Fresh Water Body Gazetteer (British Oceanographic Data Centre, 2023).

https://doi.org/10.5194/egusphere-2026-6672
Preprint. Discussion started: 25 November 2026
© Author(s) 2026. CC BY 4.0 License.

3 Methods: model inputs and application

3.1 Overview of modeling framework

To simulate shallow landslide initiation and debris-flow inundation across the study area, we developed a coupled modeling framework consisting of two components: (1) a physics-based slope stability model that estimates the spatial distribution of landslide initiation and initial failure volume, and (2) an empirical runout model, Grfin Tools, that routes these failures downslope and accounts for volumetric growth during transport (Brien et al., 2025; Cronkite-Ratcliff et al., 2025; Reid et al., 2025). The slope stability model combines slope angle, spatially variable colluvium depth, topographically derived soil wetness, soil strength, and root reinforcement to compute factor of safety (FS) for each cell of a digital elevation model (DEM). Unstable cells are then grouped into discrete landslide initiation areas, and the modeled colluvium depth is used to estimate the volume of each failure. These initiation areas and volumes are subsequently used as inputs to Grfin Tools to simulate debris-flow inundation and volumetric growth. Finally, we calibrated the runout model at the watershed scale by comparing modeled inundation with inventoried landslide extent.

Topographic analyses used a 0.5-m bare-earth digital terrain model mosaicked from two lidar acquisitions over Prince of Wales Island, collected in 2017 (Quantum Spatial, 2018) and 2018 (Quantum Spatial, 2020) and accessed through the Alaska Division of Geological & Geophysical Surveys Elevation Portal (Alaska Division of Geological & Geophysical Surveys, 2026). The mosaicked DTM and all derived rasters were resampled to 5-m resolution prior to analysis.

3.2 Spatial distribution of colluvium depth

The availability of colluvium is an important preconditioning factor for shallow landslide occurrence, as colluvium depth contributes to the gravitational driving stress required for slope failure (Parker et al., 2016). To estimate the spatial distribution of colluvium depth, we used a non-linear landscape evolution model that simulates soil production and sediment transport (Roering, 2008). Soil production decreases nonlinearly with depth, and soil transport varies nonlinearly with slope. Soil production rate, ε, is:

$$\varepsilon = \frac{\varepsilon_0}{\cos\theta} e^{-\mu h \cos\theta} \quad (1)$$

where ε_0 is the maximum soil production rate associated with zero depth, μ is the exponential decay constant, h is soil depth, and θ is slope in degrees. Flux, q_s, is:

$$q_s = \frac{-K\nabla z}{1 - (|\nabla z|/S_c)^2} \quad (2)$$

where K is the transport coefficient, ∇z is local gradient, and S_c is the critical gradient.

https://doi.org/10.5194/egusphere-2026-6672
Preprint. Discussion started: 25 November 2026
© Author(s) 2026. CC BY 4.0 License.

Values of the transport coefficient and critical gradient have not yet been constrained for Southeast Alaska, so we adopted values from the Oregon Coast Range (Table 1; Mathews et al., 2024; Roering, 2008), where the steep landscape, temperate forest, and disturbance regime closely parallel our study area. Because these parameters are uncertain for our study area, we interpret modeled colluvial depth as a relative measure of where colluvium tends to accumulate within reasonable bounds defined by observations from Southeast Alaska. Observed colluvium depths in landslide-prone areas are commonly on the order of 0.5–1 m (Gomi et al., 2004; Johnson et al., 2000; Patric and Swanston, 1968; Sidle, 1984; Swanston, 1969), so modeled colluvium depth was capped at 1.5 m, a conservative upper bound that allows for locally thicker deposits while remaining consistent with regional observations. The resulting model produced thicker colluvial deposits in convergent hollows and little to no colluvium on divergent ridges. To quantify the spatial distribution of colluvium, we calculated mean modeled colluvium depth for bins spanning both topographic slope angle and Laplacian curvature computed for each pixel of the DEM, where positive values of curvature indicate concavity (e.g., hollows and channels) and negative values indicate convex terrain features (e.g., ridgelines).

Our colluvium model does not explicitly account for glacial till, which underlies much of the terrain, but rather the redistribution of these deposits since deglaciation. Where weathered till contributes to the failure-prone mantle, as in parts of Maybeso Valley (Swanston, 1969), actual colluvium depth may exceed modeled values.

Table 1 Parameterization for the landscape evolution model used to estimate the spatial distribution of colluvium depth.

Parameter	Description	Value
ε_0	Maximum soil production rate (mm/yr)	0.3
μ	Soil production exponential coefficient (1/m)	3.0
K	Transport coefficient (m^2/yr)	0.005
S_c	Critical gradient	1.25

3.3 Groundwater conditions and topographic wetness

To characterize the close connection between elevated pore pressure and topographically controlled movement of groundwater in Southeast Alaska (Patric and Swanston, 1968; Sidle, 1984), we estimated spatial variations in pore water pressure using a relationship between median saturation ratio, m_w, and topographic wetness index, TWI, derived from measurements in a densely-instrumented sub-alpine catchment in the comparably post-glacial setting of the Alptal region of Switzerland (Rinderer et al., 2014). The findings of Rinderer et al. (2014) demonstrated links between topography and median saturation that establish an empirical basis for estimating relative saturation from TWI. However, because hillslopes in Southeast Alaska are commonly fully saturated during landslide-triggering storms, median conditions may underestimate peak pore-water pressures. Thus, modeled saturation is best interpreted as a relative measure of wetness across the landscape.

The topographic wetness index is defined as:

https://doi.org/10.5194/egusphere-2026-6672
Preprint. Discussion started: 25 November 2026
© Author(s) 2026. CC BY 4.0 License.

$$TWI = \ln\left(\frac{a}{\tan\beta}\right) \quad (3)$$

where a is upslope contributing area and β is local slope angle (Beven and Kirkby, 1979; Quinn et al., 1995). To estimate the saturation ratio used in Equation (5), we fit a logistic function to the relationship between TWI and median saturation from (Rinderer et al., 2014):

$$m_w(TWI) = \frac{L}{1 + e^{-k(TWI - TWI_0)}} \quad (4)$$

where TWI_0, L, and k are fitting parameters. The fitted relationship was then applied to every DEM pixel, assigning a median saturation ratio (m_w) as a continuous function of TWI, with values ranging from 0 to 1. This approach does not account for storm-driven temporal variation in soil saturation that models such as TRGRS (Baum et al., 2008) generate but rather captures a representative elevated soil saturation condition and its spatial variation.

3.4 Soil and root reinforcement parameters

We derived spatial distributions of soil shear strength parameters by applying geotechnical measurements from Southeast Alaska (Filz, 1981; Schroeder, 1983; Schroeder and Swanston, 1987) to soil map units from the Tongass National Forest Soil Resource Inventory (Fig. S1a; U.S. Forest Service, 2020). Mean values of effective friction angle (ϕ'), effective cohesion (c'), and bulk unit weight (γ) were assigned to each mapped soil series using results from triaxial testing and field measurements collected at 40 sites throughout Southeast Alaska (Table 2). Although this sample size is limited and only eight of the samples are from Prince of Wales Island, representative soil testing would be resource intensive and impractical at the spatial scale of our study area. To further estimate the distribution of geotechnical parameters, future studies could potentially utilize geotechnical back-analysis of known landslides to characterize shear strength and associated uncertainty (Alberti et al., 2022; Bunn et al., 2020a, b; Gong et al., 2023; Mathews et al., 2024).

Several soil series mapped within the study area lacked corresponding geotechnical measurements. For these series, we sampled soil series at TNFLI landslide initiation points and identified the soil series most frequently associated with mapped landslides. We assigned the corresponding geotechnical parameters to unrepresented soil series and areas without soil-series mapping (Fig. S1a). This approach ensured complete spatial coverage of geotechnical parameters while using values from a soil series frequently associated with shallow landslides in the region.

We assumed that roots contribute 4.9 kPa to shear strength, treated as effective cohesion in Equation (5). This value corresponds to the average tensile strength of roots in virgin forests measured within the Maybeso Valley, but tensile strength may be substantially lower in areas of previous timber harvest (Sidle, 1991; Wu et al., 1979).

https://doi.org/10.5194/egusphere-2026-6672
Preprint. Discussion started: 25 November 2026
© Author(s) 2026. CC BY 4.0 License.

Table 2 Mean soil parameters for soil series present in the study area.

TNF Code	Series Name	Mean ϕ' (°)	Mean c' (kPa)	Mean γ[1] (kN/m^3)
KAT	Karta	36	7	19
TOK	Tokeen	36	5	16
ULL	Ulloa	34	6	16
WAD	Wadleigh	37	9	19
KUP	Kupreanof	38	9	17
TRA	Traitors	36	10	16
TOL	Tolstoi	36	7	17

[1] Schroeder & Swanston (1987) reports these values simply as mean unit weight in their slope stability analysis. We assume them to be mean bulk unit weights and do not differentiate between dry and saturated unit weights in this study.

3.5 Slope stability, landslide initiation, and validation

We used a physics-based limit equilibrium model to assess slope stability. Given the shallow nature of the landslides considered in this study, we used the infinite slope model to evaluate factor of safety, FS (Taylor, 1948):

$$FS = \frac{c + s_r}{\gamma z \sin\theta} + \frac{\tan\phi}{\tan\theta}\left(1 - m_w \frac{\gamma_w}{\gamma}\right) \quad (5)$$

where c is apparent cohesion, s_r is root reinforcement, γ is the bulk unit weight of colluvium, z is depth to the failure plane, θ is slope angle, ϕ is the angle of internal friction, m_w is the saturation ratio (the ratio of saturated water height to z), and γ_w is the unit weight of water. Because the unsaturated behavior of soils in Southeast Alaska remains poorly understood, we assumed that c represents all contributions to normal-stress-independent shear strength, including mineral cohesion, root reinforcement, and stresses associated with moisture-dependent processes (Lu and Likos, 2013).

We calculated FS for every DEM pixel using topographic slope, estimated saturation ratio, modeled colluvium depth, and spatially distributed soil parameters. Pixels with $FS \leq 1$ were classified as unstable and pixels with $FS > 1$ were considered stable. We identified clusters of interconnected unstable pixels as discrete landslides using an 8-pixel connected-components algorithm in MATLAB (Alvioli et al., 2014; Mathews et al., 2024). Because each pixel has a corresponding colluvium depth, the total volume for a given landslide is the sum of volumes for all interconnected pixels (Bellugi et al., 2015; Mathews et al., 2024).

We evaluated initiation-model performance across the entire study area by assessing its ability to distinguish between stable and unstable terrain when compared to the TNFLI landslide initiation inventory. To do this, we used receiver operating characteristic (ROC) analysis and the corresponding area under the curve (AUC). Following Patton et al. (2022), we assessed model skill based on its ability to distinguish mapped landslide initiation points from randomly generated non-landslide locations. Landslide initiation points were obtained from the TNFLI (U.S. Forest Service, 2024b) and clipped to the DEM

https://doi.org/10.5194/egusphere-2026-6672
Preprint. Discussion started: 25 November 2026
© Author(s) 2026. CC BY 4.0 License.

boundary (n = 1,243). Because TNFLI landslide locations may contain positional uncertainty on the order of 10 m (Patton et al., 2022), we applied a 10-m radius buffer to each initiation point, and the minimum value of FS within this buffer was extracted to characterize local instability conditions. Stable conditions were represented by 5,000 randomly generated points restricted to terrestrial areas within the study area. Following Patton et al. (2022), non-landslide points were limited to terrain steeper than 25°. To account for variability in non-landslide point sampling, reported AUC values represent the mean from 20 independent trials of 5,000 background points. To compare performance for various model parameterizations, we also calculated ROC curves and mean AUC values for a range of uniformly distributed colluvium depths and saturation ratios.

To construct the ROC curve, we systematically varied the threshold of FS defining unstable conditions across the range of modeled FS values. While FS values greater than one do not physically indicate slope instability because the forces resisting landslide initiation exceed those driving it, this approach enabled us to test the model's ability to distinguish stable and unstable terrain across the range of modeled FS values. For each threshold value, the true positive rate and false positive rate were calculated and plotted to generate the ROC curve. The area under the curve (AUC) is a threshold-independent measure of binary classification performance and, in this study, the model's ability to distinguish stable from unstable terrain. Although no universal standard exists for interpreting AUC values, Hosmer et al. (2013) suggested that AUC values between 0.7 and 0.8 reflect acceptable discrimination, values between 0.8 and 0.9 signify excellent discrimination, and a value of 0.5 represents performance equivalent to random guessing.

3.6 Runout modeling and volumetric growth

We simulate debris-flow inundation using Grfin Tools, a software package developed by the U.S. Geological Survey (USGS) for modeling runout from debris flows, lahars, and other slope failures (Brien et al., 2025; Cronkite-Ratcliff et al., 2025). Notably, Grfin Tools accounts for entrainment that can significantly increase debris-flow volume and influence inundation area in debris-flow-prone, soil-mantled landscapes (Burns et al., 2025; Reid et al., 2016; Scheip and Wegmann, 2022).

To limit debris-flow initiation to unstable locations within the landscape and capture associated initial volumes, we used the landslide initiation locations and volumes generated by our slope stability framework as inputs to Grfin Tools. We defined the initiation point for each modeled landslide as the highest-elevation pixel within its initiation area (i.e., cluster of failed pixels). When defining modeling options within Grfin Tools, we implemented the *inundation* and *growth* options to simulate landslide runout, where cross-sectional area, A, and planimetric inundation area, B, are related empirically to volume, V:

$$A = \alpha V^{2/3} \quad (6)$$

$$B = \beta V^{2/3} \quad (7)$$

https://doi.org/10.5194/egusphere-2026-6672
Preprint. Discussion started: 25 November 2026
© Author(s) 2026. CC BY 4.0 License.

where α and β are empirical coefficients describing cross-sectional and planimetric inundation area, respectively. We also used the *hbar* option which enforces a minimum inundation depth and limits the planimetric spread of debris flow deposits (Reid et al., 2025).

Growth zones are defined as portions of the modeled stream network where debris-flow volume is increased during transport by a specified volumetric growth factor. Within Grfin Tools, volumetric growth can be a function of either upstream stream length or contributing area. Because debris flows in the region increase volume by entraining colluvium in steep channels during transport, we assume volumetric growth to be proportional to upstream stream length. Growth zones were defined using a stream gradient threshold that separates net deposition from erosion, referred to as the *transition slope angle* hereafter (Johnson et al., 2000; Reid et al., 2016).

In Version 1.0, Grfin Tools initiates debris flows from all growth zones within the DEM, regardless of whether a user-defined initiation point exists upstream. To restrict debris-flow initiation to locations identified by our initiation framework, we limited growth zones to channels downstream of modeled initiation points. First, we generated a stream network using the default parameters in Grfin Tools and rasterized it to match the DEM extent and resolution. Second, we simulated runout from all modeled initiation points using an unrealistically high value of β ($\beta = 80$) to conservatively delineate all potential flow paths. Third, we defined growth zones as stream-network pixels within the exaggerated inundation paths that exceeded the transition slope angle. The resulting growth zones therefore included only channels reachable by debris flows originating from modeled initiation locations, which prevented initiation in channels not downstream of modeled shallow landslides while ensuring that potential growth zones were not omitted.

3.7 Runout parameterization and calibration

To quantify potential spatial variability in runout behavior, we calibrated the transition slope angle and volumetric growth factor in Grfin Tools against inventoried debris flows at the watershed scale. We partitioned the DEM into HUC-14 watersheds and calibrated each one independently. For each watershed, we evaluated three transition slope angles (15°, 20°, and 25°), informed by field measurements from Johnson et al. (2000), and six volumetric growth factors ranging from 5-30 m^3/m by comparing modeled inundation originating at TNFLI initiation points to the TNFLI inundation areas. For all simulations, we adopted runout coefficients of α = 0.11 and β = 8.0. These values were developed specifically for Southeast Alaska by Booth et al. (2020) to reflect lower mobility than globally derived coefficients because debris-flow runout in Southeast Alaska is inhibited by the entrainment of large woody debris.

Grfin Tools produces a raster of inundated cells that does not distinguish individual debris flows, making individual landslide validation and testing with the inventory untenable. Instead, to evaluate how well modeled debris flows agree with those from the TNFLI, we assess spatial similarity at the watershed scale using the similarity index (Heiser et al., 2017), following the approach of Gorr et al. (2022). We constructed a confusion matrix for each watershed, defining true positives (TP), false positives (FP), and false negatives (FN), which we then used to compute similarity index:

https://doi.org/10.5194/egusphere-2026-6672
Preprint. Discussion started: 25 November 2026
© Author(s) 2026. CC BY 4.0 License.

$$SI = \alpha_T - \beta_T - \gamma_T \quad (8)$$

where $\alpha_T = TP/(TP + FP + FN)$, $\beta_T = FN/(TP + FP + FN)$, and $\gamma_T = FP/(TP + FP + FN)$. Here, α_T represents areas where modeled and inventoried debris flows overlap, and β_T and γ_T indicate areas of model underestimation and overestimation, respectively. Values range from −1 to 1, where 1 indicates perfect agreement and values below 0 indicate that errors exceed correctly predicted inundation.

Grfin Tools requires a volume associated with each initiation point, which the TNFLI does not provide. To estimate initiation volume for each inventoried initiation, we first estimated debris-flow volumes from full TNFLI landslide areas using the empirical area-volume relationship $V_L = 1.0359{A_L}^{0.880}$, derived from 615 landslides on nearby Haida Gwaii (Guzzetti et al., 2009; Martin et al., 2002). We then estimated the initial-volume fraction by scaling a histogram of TNFLI volumes by a scaling factor, f_V, until it best-matched a histogram of volumes computed using the initiation framework. The optimal scaling factor was determined using least-squares minimization,

$$LS = \sum_{i=1}^{n} \left(f_V * P_{inventory,i} - P_{model,i}\right)^2 \quad (9)$$

where $P_{inventory,i}$ and $P_{model,i}$ are probabilities of volumes for bin i, for the TNFLI and modeled landslides, respectively, and is the total number of volume bins. Initiation volume was then computed for each slide:

$$V_{initiation} = f_V * V_L \quad (10)$$

Finally, using these estimated initiation volumes associated with the TNFLI, we evaluated combinations of volumetric growth factors and transition slope angles within each HUC-14 watershed and selected the parameter values that maximized the similarity index.

4 Results

4.1 Topographic relationships with colluvium depth

The landscape evolution model predicted deeper colluvium within convergent hollows and shallow to absent colluvium on divergent terrain features. Mean colluvium depth increased with binned values of Laplacian curvature within the range of

https://doi.org/10.5194/egusphere-2026-6672
Preprint. Discussion started: 25 November 2026
© Author(s) 2026. CC BY 4.0 License.

approximately -0.05 to 0.15 m^{-1} (Figure 3a). However, for curvature values greater than about 0.15 m^{-1}, mean colluvium depth declines with increasing curvature, while the standard deviation of colluvium depth within each bin increases.

Consequently, locations with high curvature but different slope angles can exhibit substantially different colluvium depths. In Figure 4, point A shows a steep mountain channel that, despite very high curvature (1.42 m^{-1}), hosts no colluvium due to its very steep slope angle (80°) that promotes high sediment flux. Point B illustrates another channel with curvature exceeding that of 99.9% of pixels within the DEM (0.39 m^{-1}). At a slope angle of 40°, it is both gentle enough for colluvium to accumulate (1.1 m) and steep enough to promote landsliding. Point C has curvature high enough (0.19 m^{-1}) to accumulate thick colluvium (1.5 m) but its relatively gentle slope angle of 27° makes landslide initiation unlikely. Point D represents relatively moderate curvature (0.17 m^{-1}) on a 33°, unchannelized hillslope, yielding 0.3 m of colluvium. Landslides on Prince of Wales Island most commonly originate on slopes ranging from 30° to 50°, but can also originate on gentler slope areas, especially in clearcut areas (Johnson et al., 2000; Swanston, 1969).

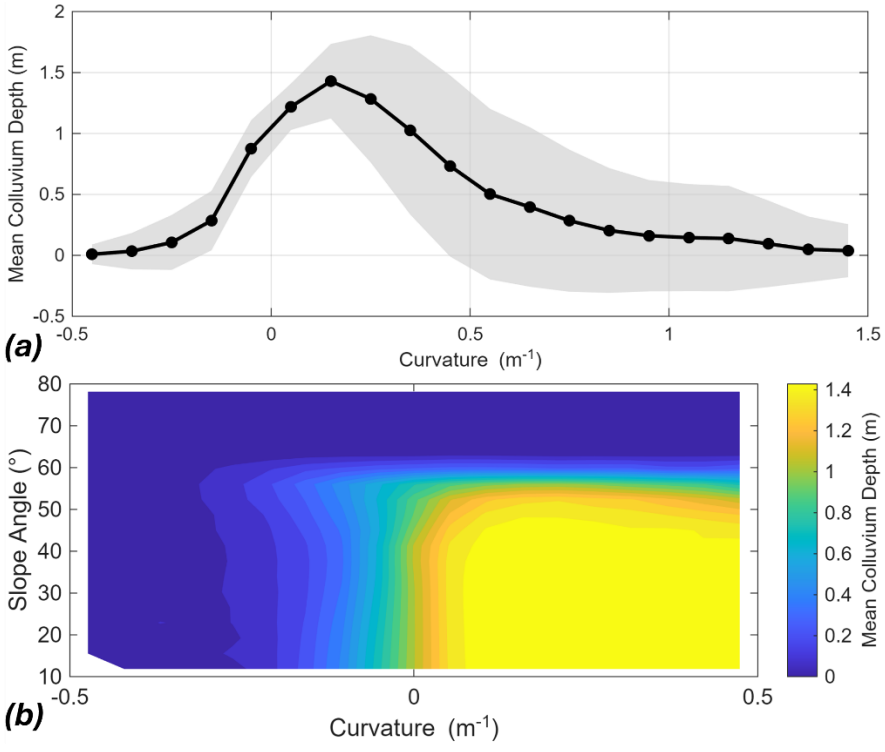

Figure 3 Relationships between modeled colluvium depth, Laplacian curvature, and slope angle: (a) Mean colluvium depth and ±1 standard deviation (gray shading) across curvature bins. (b) Mean modeled colluvium depth as a function of curvature and slope angle.

https://doi.org/10.5194/egusphere-2026-6672
Preprint. Discussion started: 25 November 2026
© Author(s) 2026. CC BY 4.0 License.

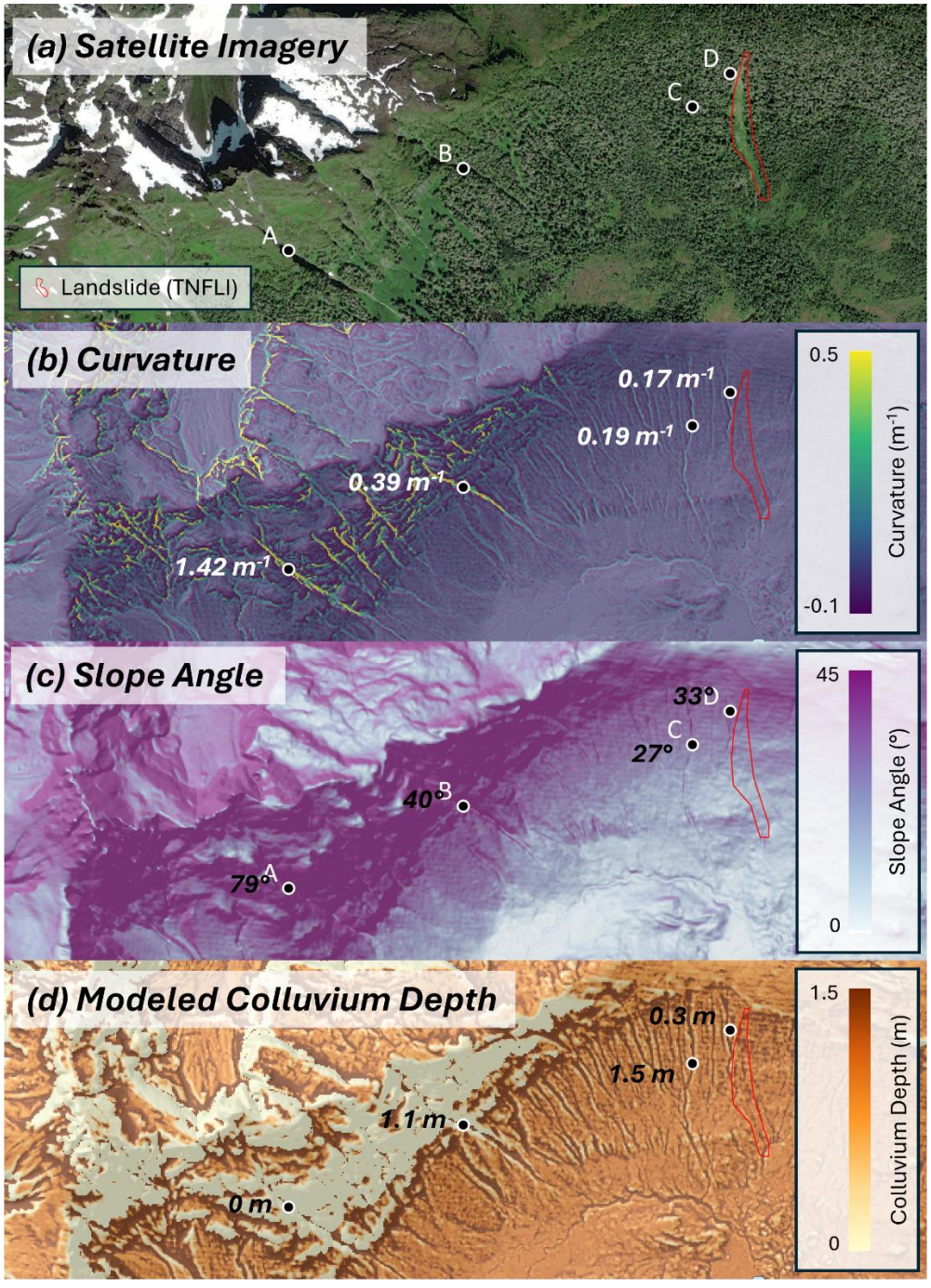

Figure 4 Curvature, slope angle, and corresponding colluvium depths from four locations on a steep hillslope. Point A shows a steep mountain channel that, despite very high curvature (1.42 m^{-1}), hosts no colluvium due to its very steep slope angle (80°) promoting high sediment flux. Point B illustrates another channel with curvature exceeding that of 99.9% of pixels within the DEM (0.39 m^{-1}). It is convergent and steep enough (40°) that landslides are possible, but the angle is gentle enough to support 1.1 m of colluvium. Point C has curvature high enough (0.19 m^{-1}) to accumulate thick colluvium (1.5 m) but its relatively gentle slope angle of 27° makes landslide initiation unlikely. Point D represents relatively moderate curvature (0.17 m^{-1}) on a 33°, unchannelized hillslope, yielding 0.3 m of colluvium. Satellite imagery in (a):

https://doi.org/10.5194/egusphere-2026-6672
Preprint. Discussion started: 25 November 2026
© Author(s) 2026. CC BY 4.0 License.

Esri, Maxar, Earthstar Geographics, and the GIS User Community | Powered by Esri. Hillshade derived from lidar (Quantum Spatial, 2018, 2020).

4.2 Topographically derived groundwater conditions

Fitting Equation (4) to data from Rinderer et al. (2014) yielded a nonlinear relationship between TWI and m_w that we used to estimate pore-water pressure throughout the study area (Figure 5; $R^2 = 0.61$). Convergent topography with large contributing areas and gentle slopes yielded higher TWI values, resulting in higher pore pressures. In contrast, low TWI values were associated with divergent terrain and steep slope angles that promote rapid drainage, resulting in lower pore pressures.

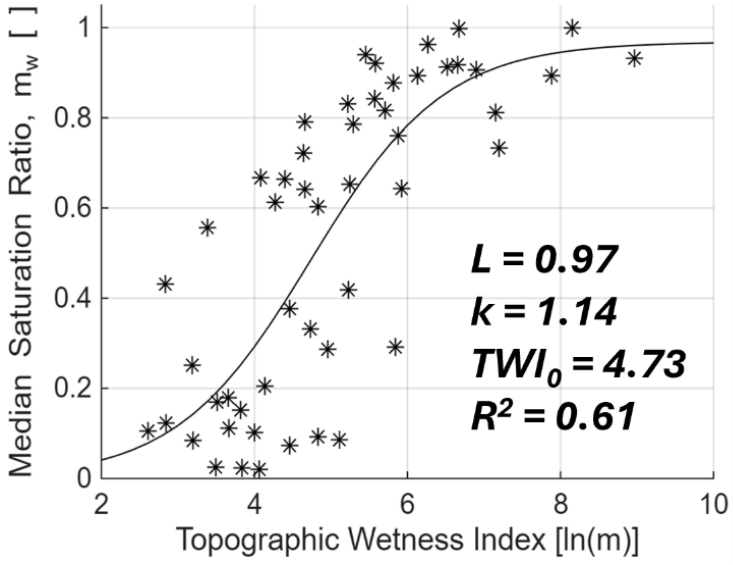

Figure 5 Logistic function fit to topographic wetness index and median saturation ratio data from Rinderer et al. (2014).

4.3 Landslide initiation: validation and spatial patterns

The slope stability model produced the lowest factors of safety within steep, convergent colluvial hollows where both colluvium depth and saturation were greatest, resulting in localized zones of instability instead of vast swaths of instability across steep terrain. Within terrain with slope angles ranging 35° to 45°, full saturation ($m_w = 1$) alone did not produce instability ($FS \leq 1$); rather, factor of safety decreased primarily with colluvium depth, indicating that sufficient colluvium preconditions slopes for failure. (Figure 6).

The landslide initiation model with modeled colluvium depth and TWI-based saturation achieved an AUC of 0.855 when compared with TNFLI initiation points, indicating excellent discrimination between landslide and non-landslide locations and the best performance among the parameterizations tested (Figure 7a; solid blue curve). Modeled colluvium scenarios yielded the highest AUC for all saturation conditions (Figure 7b). Additionally, for all colluvium-depth scenarios, TWI-based saturation produced higher AUC values than all uniform saturation models. Compared to the full suite of uniform depth and

https://doi.org/10.5194/egusphere-2026-6672
Preprint. Discussion started: 25 November 2026
© Author(s) 2026. CC BY 4.0 License.

saturation models, accounting for the spatial distributions of colluvium and saturation improved model AUC by 0.059-0.097. Finally, ROC curves show that for a given true positive rate, models with modeled colluvium depth demonstrate lower false positive rates than those with uniform colluvium (Figure 7a). This reflects the ability of our model to distinguish unstable terrain within steep hillslopes instead of characterizing broad swaths of steep terrain as unstable, resulting in high a high rate of false positives.

These scenarios produced markedly different spatial patterns of instability at $FS = 1$, a physically meaningful threshold at which driving and resisting forces are equal and incipient failure occurs (Figure 8). Uniform colluvial depths produced bands of instability (deep red) that generally followed topographic contours along the steepest parts of the landscape, and instability became more widespread with deeper colluvial depth and higher saturation. Conversely, modeling both colluvium depth and TWI-based saturation constrained failure areas to discrete colluvial hollows.

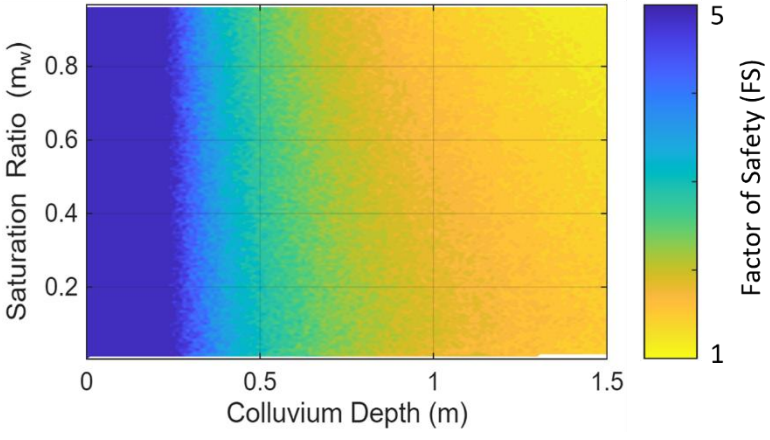

Figure 6 Contour map of factor of safety as a function of colluvium depth and saturation ratio (m_w) for all pixels with slope angles between 35° and 45°.

https://doi.org/10.5194/egusphere-2026-6672
Preprint. Discussion started: 25 November 2026
© Author(s) 2026. CC BY 4.0 License.

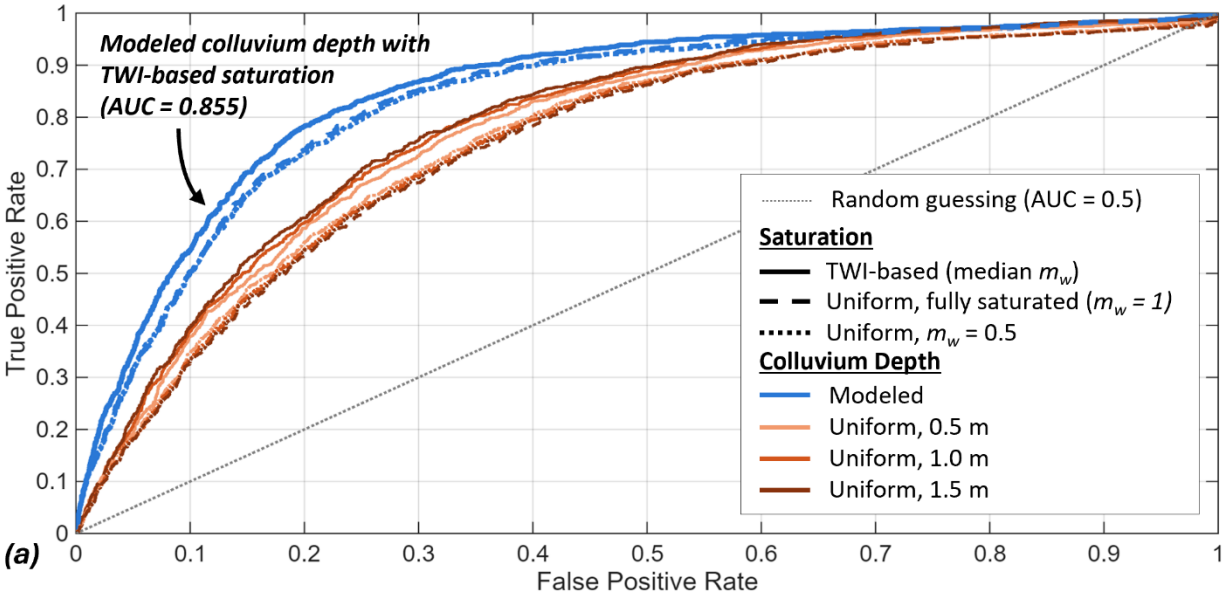

(b) Mean AUC for All Scenarios

Colluvium Depth \ Saturation	Uniform, m_w = 0.5	TWI-based (median m_w)	Uniform, fully saturated (m_w = 1)
Modeled	0.838	0.855	0.840
Uniform, 0.5 m	0.768	0.783	0.767
Uniform, 1.0 m	0.764	0.791	0.762
Uniform, 1.5 m	0.761	0.796	0.758

AUC: 0.85, 0.8, 0.75

Figure 7 (a) ROC curves comparing factor of safety at TNFLI initiation points with random background points on slopes ≥ 25° for modeled and uniform colluvium depths (0.5, 1.0, 1.5 m), and TWI-based saturation and uniform saturation conditions (m_w = 0.5 and m_w = 1.0). (b) Mean AUC for each scenario.

https://doi.org/10.5194/egusphere-2026-6672
Preprint. Discussion started: 25 November 2026
© Author(s) 2026. CC BY 4.0 License.

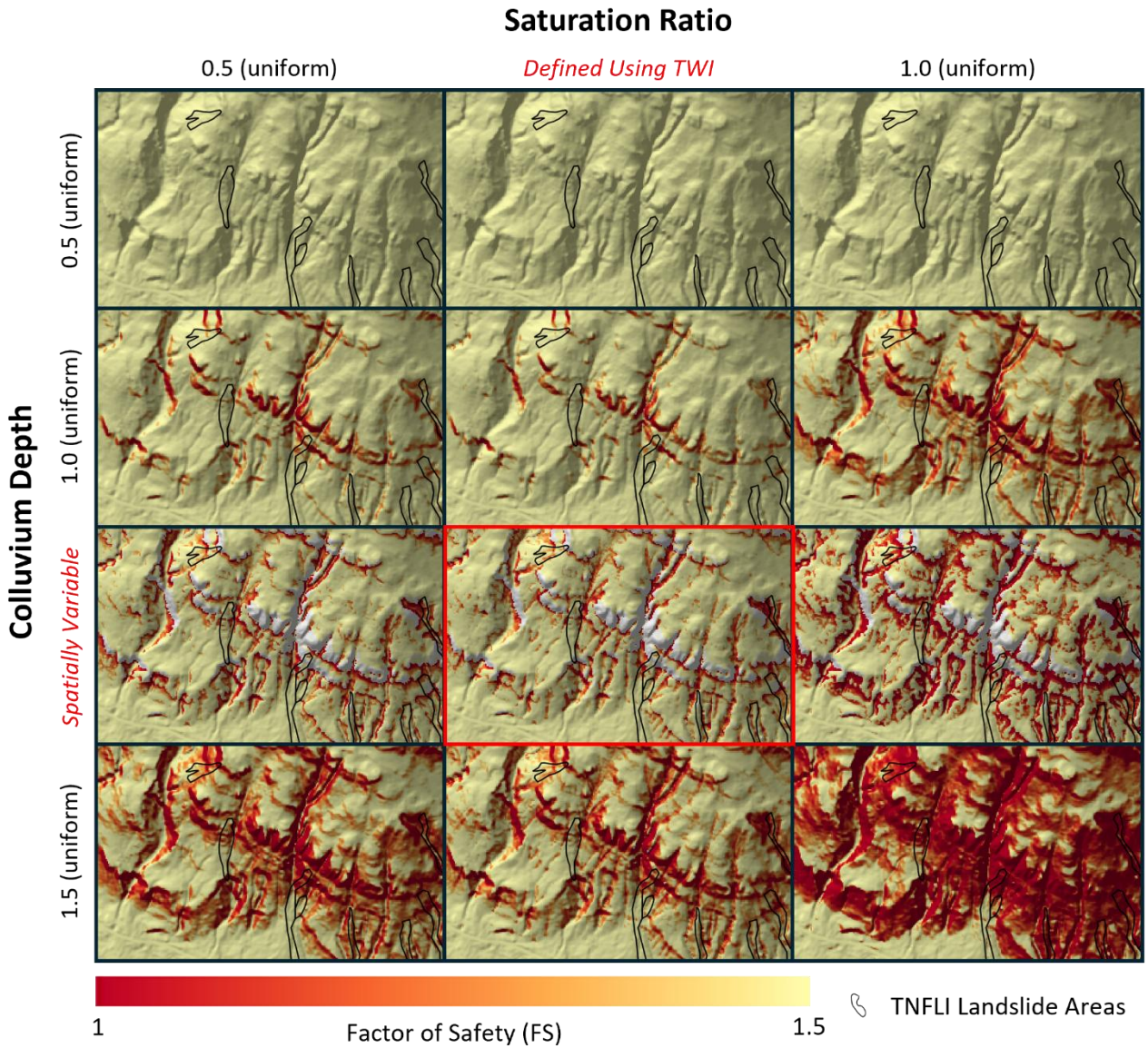

440 Figure 8 Factor of safety for combinations of colluvium depth (rows) and saturation conditions (columns) for an example portion of the study area. Deep red indicates FS ≤ 1, TNFLI landslide areas are outlined in black, and unshaded areas represent modeled colluvium depth of zero. Hillshade derived from lidar (Quantum Spatial, 2018, 2020).

4.4 Runout modeling and calibration

To quantify spatial variability in debris flow behavior, we calibrated Grfin Tools independently within each of the 120 445 HUC-14 watersheds using the TNFLI. Through least-squares minimization, scaling TNFLI landslide volumes by 0.07 produced optimal agreement with modeled initiation volumes (R^2 = 0.97; Fig S2). This scaling factor indicates that initiation volumes comprise approximately 7% of the final debris-flow volume within the study area.

https://doi.org/10.5194/egusphere-2026-6672
Preprint. Discussion started: 25 November 2026
© Author(s) 2026. CC BY 4.0 License.

Of the 120 watersheds, 87 contained at least one inventoried landslide producing a similarity index corresponding to optimal transition slope and volumetric growth factor with no consistent spatial pattern in the optimal parameter combinations (Figure **9**). Similarity indices showed no obvious spatial pattern across the study area. Among the 87 watersheds, the mean similarity index was -0.38 ($\sigma = 0.18$) with minimum and maximum values of -0.76 and 0.41, respectively. Similarity indices were mostly between -0.6 to -0.2, and all watersheds with similarity indices greater than -0.2 contained fewer than four inventoried landslides (Fig. S3). Similarity indices generally decreased as the heterogeneity of inventoried debris-flow mobility within a single watershed increased. Heterogeneity was quantified as the coefficient of variation (CV) of H/L (landslide fall height normalized by runout length) within each watershed (Section 1.3 of the Supplementary Information; Fig. S3).

Figure 10 illustrates the outcome of the calibration procedure for an area containing two adjacent watersheds (extent shown by red bounding box in Figure 9). Growth zones generated using transition slopes ranging from 15-25° (Figure 10a) were combined with volumetric growth factors ranging from 5-30 m^3/m to identify the parameter combination that maximized the similarity index (Figure 10b). For the western watershed, the optimal transition slope was 25° and the optimal volumetric growth factor was 10 m^3/m. For the eastern watershed, the optimal transition slope was 25° and the optimal volumetric growth factor was 30 m^3/m. Modeling using these calibrated parameters generated many debris flows overlapping with TNFLI landslide areas, while also identifying potential debris-flow paths in areas without inventoried landslides (Figure 10c). A full suite of maps showing inundation susceptibility are shown in the repository referenced in the code and availability statement (Mathews and Roering, 2026).

https://doi.org/10.5194/egusphere-2026-6672
Preprint. Discussion started: 25 November 2026
© Author(s) 2026. CC BY 4.0 License.

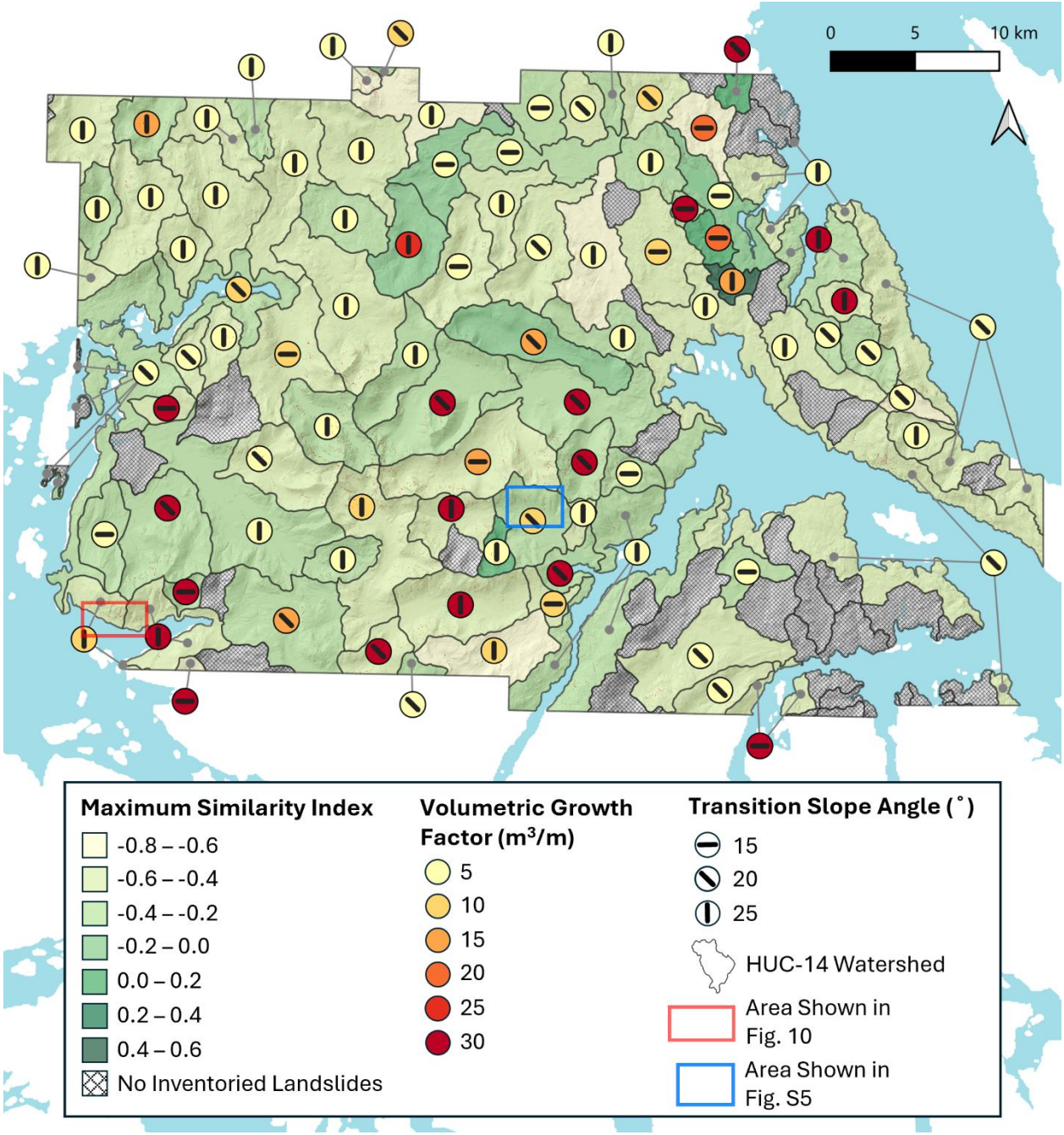

Figure 9 Map of runout modeling parameters, calibrated through comparison to TNFLI landslides: similarity index, volumetric growth factor, and transition slope angle. Parameter shading corresponds to the maximum similarity index (i.e., best performance) for the parameter suite tested. Black lines coming out of volumetric growth factor and transition slope angle markers point to disconnected watersheds corresponding to the marker. Some watersheds are discontinuous due to bodies of water separating them or from clipping them to the study area domain. Hillshade derived from lidar (Quantum Spatial, 2018, 2020). Water bodies from the SeaVoX Salt and Fresh Water Body Gazetteer (British Oceanographic Data Centre, 2023).

https://doi.org/10.5194/egusphere-2026-6672
Preprint. Discussion started: 25 November 2026
© Author(s) 2026. CC BY 4.0 License.

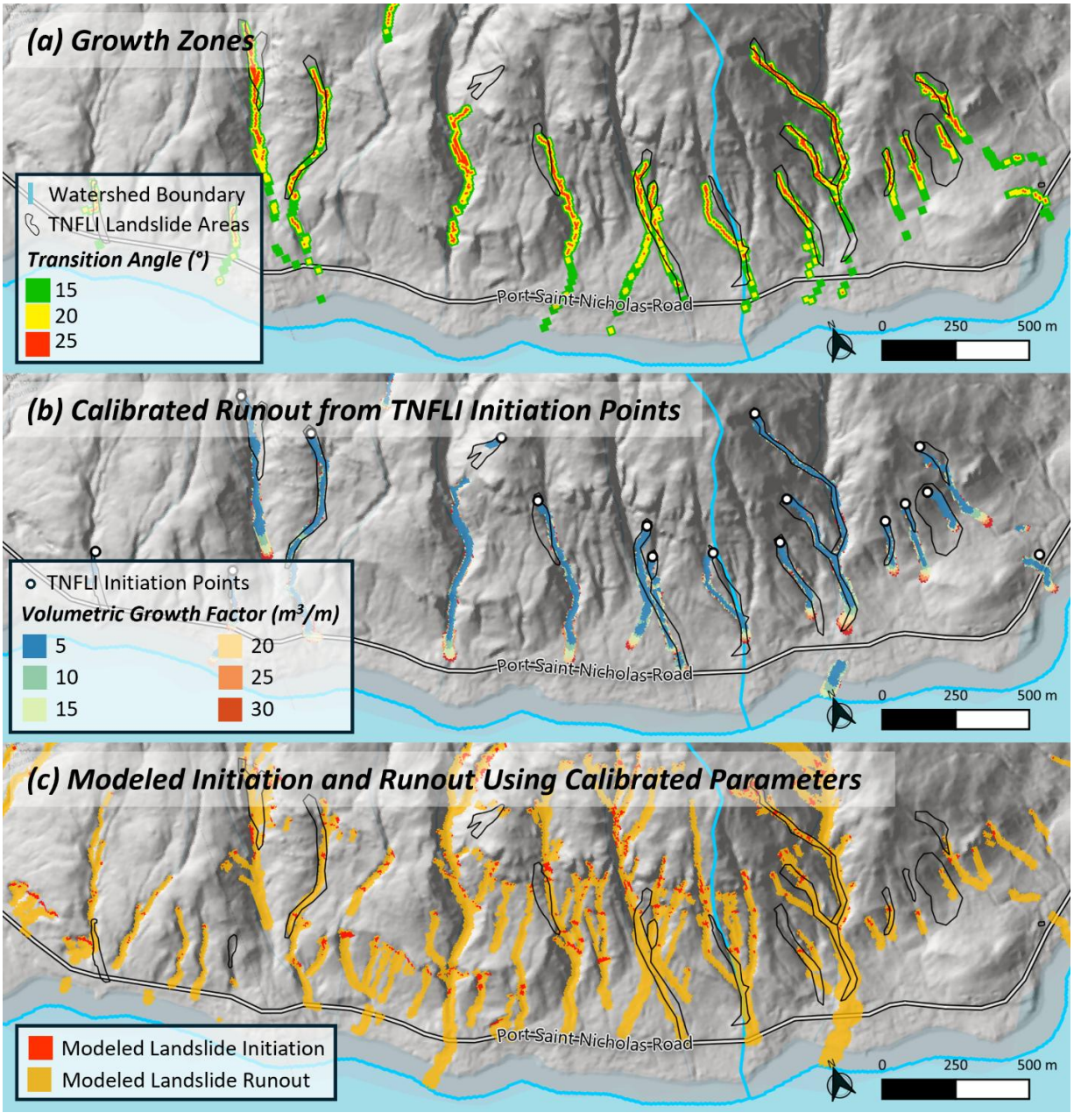

Figure 10 Map of debris flow growth zones, initiation and runout above Port Saint Nicholas, a debris-flow prone region east of Craig, AK (area extent shown in Figure 9). The optimal calibrated volumetric growth factor and transition angle are 10 m^3/m and 25° for the western watershed and 30 m^3/m and 25° for the eastern watershed (separated by light blue watershed boundary; calibrated values shown in in Figure 9). (a) Example of growth zones generated for inventories debris flow paths for transition angles of 15°, 20°, and 25°. (b) Modeled runout using the optimized transition slope and a range of volumetric growth factors originating at TNFLI initiation points. Volumes assigned to the initiation points are 7% of total volume as determined using the area-volume relationship from Haida Gwaii and the optimal volume scaling factor, f_v. (c) Modeled initiation from the slope stability model and corresponding runout using calibrated volumetric growth factor and transition angle. Hillshade derived from lidar (Quantum Spatial, 2018, 2020). Road data © OpenStreetMap contributors (openstreetmap.org/copyright). Water bodies from the SeaVoX Salt and Fresh Water Body Gazetteer (British Oceanographic Data Centre, 2023).

https://doi.org/10.5194/egusphere-2026-6672
Preprint. Discussion started: 25 November 2026
© Author(s) 2026. CC BY 4.0 License.

5 Discussion

5.1 Process-scale controls on landslide initiation susceptibility

Our results demonstrate that accounting for variable colluvium depth by modeling soil production and flux, and computing saturation based on TWI, improved the performance of the landslide initiation model. This distinction is important in areas like Southeast Alaska, where steep terrain is widespread and models based primarily on slope, relief, or other first-order terrain metrics may conservatively identify large portions of the landscape as susceptible, resulting in a high rate of false positives. In contrast, our physics-based initiation framework simulates processes that control colluvium accumulation and hydrologic convergence. Thus, steep, convergent hollows were preferentially identified as unstable while adjacent, divergent terrain with similar slope angle commonly remained stable (Figure 8).

The high AUC of the initiation model with modeled colluvium depth and TWI-based saturation (0.86) demonstrates that this process-based parameterization can skillfully distinguish inventoried landslide points from non-landslide locations in steep terrain while producing lower false positive rates than models that assume uniform distributions of these parameters (Figure 7a). Using the classification of Hosmer et al. (2013), only models with modeled colluvium achieved “excellent” discrimination ($0.8 \leq AUC < 0.9$), while uniform-depth models performed, at best, in the “acceptable” range ($0.7 \leq AUC < 0.8$; Figure 7b). This behavior differs from regional susceptibility approaches that rely primarily on first-order topographic metrics (Mirus et al., 2024) or that do not account for topographically driven heterogeneity in colluvium depth and saturation (Nicolazzo and Larsen, 2025; Salisbury, 2024), which are useful for identifying broad areas elevated susceptibility but may have limited ability to distinguish stable and unstable terrain on the sub-hillslope scale. For reference, Fig. S4 compares the spatial patterns of the only other publicly available susceptibility map – the USGS National Susceptibility Map – to a factor of safety map from this study.

The importance of these controls is consistent with Dietrich et al. (1995), in which topography, soil depth, and hydrology all interact to produce the spatial pattern of landslide initiation potential. Our results indicate that fully saturated conditions do not necessarily cause slope failure where colluvium is thin or absent; instead, increasing saturation progressively reduces factor of safety where sufficient colluvium is present, producing the greatest potential for instability where thick colluvium and elevated saturation coincide (Figure 6). Thus, the modeling results reflect the hypothesis that colluvium availability establishes the conditions for failure (Parker et al., 2016), while rainfall capable of producing sufficient pore-water pressure acts as the landslide trigger (Baum et al., 2010; Terzaghi, 1950).

Explicitly modeling soil production and transport to calculate colluvium depth carries some unique advantages (e.g., Dietrich et al., 1995). Many existing regional-scale slope stability frameworks either assume uniform soil depth (e.g., Kassem & Zekkos, 2026), evaluate a range of depths to identify a critical failure depth (Baum et al., 2008, 2010), or define soil depth empirically as a function of slope, elevation, and/or curvature (Catani et al., 2010; Pollock and Wartman, 2026). The landscape

https://doi.org/10.5194/egusphere-2026-6672
Preprint. Discussion started: 25 November 2026
© Author(s) 2026. CC BY 4.0 License.

evolution model used herein demonstrates that colluvium depth increases with curvature, but departs from that pattern and begins to decrease at curvature values higher than 0.15 m^{-1} (Figure 3a). We attribute this pattern to the presence of steep midslope channels where, despite high curvature and convergence, the nonlinear flux term (2) produces downslope sediment transport exceeding soil production, preventing colluvium from accumulating within very steep terrain (Figure 3b). This indicates that curvature alone becomes a poor predictor of colluvium depth where steep slope angles may strongly influence sediment transport.

The influence of topography on groundwater conditions is an important consideration for shallow landslide susceptibility. We estimated saturation from topographic wetness rather than assuming spatially uniform groundwater conditions which captured the tendency for subsurface water to converge in topographic hollows (Beven and Kirkby, 1979; Dietrich et al., 1995). Although the TWI-saturation relationship was derived from an instrumented catchment outside of Southeast Alaska, its resulting hydrological patterns contributed to the spatial differentiation between unstable, convergent terrain and relatively stable divergent terrain (Figure 8). Hydrologic conditions can change over timescales of hours to days during rainfall events (Iverson, 2000), while colluvium accumulates over hundreds to thousands of years in humid, forested environments (Parker et al., 2016; Wu et al., 1979). However, the approach herein models saturation as a static condition, and the resulting maps should therefore be interpreted as static susceptibility maps representing the relative likelihood of landslide initiation. Transient infiltration models used in slope-stability frameworks can capture temporal changes in pore pressure, but are often one-dimensional and do not capture the topographic patterns of saturation (Baum et al., 2008, 2010; Iverson, 2000). Combining colluvium distributions derived from production and flux with spatially distributed, transient infiltration in physics-based slope-stability modeling (e.g., Moon et al., 2026) could potentially expand this framework toward storm-based hazard modeling.

5.2 Data-sparse calibration of regional-scale debris-flow inundation

Predicting debris-flow inundation on broad spatial scales remains challenging because the processes governing debris-flow mobility are spatially heterogenous and difficult to quantify (McDougall, 2017). Debris-flow runout depends on complex interactions between sediment availability, entrainment, channel morphology, vegetation, fluid–solid interactions, and flow rheology (Booth et al., 2020; Iverson, 1997; Reid et al., 2016). Process-based models can capture these mechanisms explicitly but are difficult to implement at the regional scale because they require extensive parameterization and are computationally demanding. Alternatively, regional-scale assessments often apply empirical runout models (e.g., Brien et al., 2025; Burns et al., 2022; Nicolazzo & Larsen, 2025) These models are computationally efficient but typically assume a single set of parameters across a large landscape and may not capture the spatial variability in debris-flow mobility across watersheds.

Our results demonstrate an alternative approach in which physically meaningful parameter ranges constrained from literature are further optimized through comparison to inventoried landslide areas at the watershed scale. This approach maintains the efficiency and minimal data requirements of an empirical runout model while still capturing differences in debris-flow characteristics across the landscape (Figure 9). This is particularly useful in regions like Southeast Alaska, where an

https://doi.org/10.5194/egusphere-2026-6672
Preprint. Discussion started: 25 November 2026
© Author(s) 2026. CC BY 4.0 License.

extensive landslide inventory exists but direct measurements of debris-flow behavior, including flow depth, velocity, and event-scale changes in channel morphology from multitemporal lidar or field observations, are sparse.

The Southeast-Alaska-specific area-volume relationships from Booth et al. (2020) yielded reasonable agreement between modeled inundation areas and TNFLI landslide areas within a physically plausible set of transition slope angle and volumetric bulking factor parameters (Figure 10c). The calibrated simulations generally reproduced the scale and width of the inventory landslides and predicted debris flow activity where landslides observations are dense, but inundation was underestimated in some notable areas, namely the Maybeso Valley northwest of Hollis, AK. We hypothesize that this stems from land use history, specifically extensive timber harvest in 1955 and 1958 that was followed by widespread landsliding in 1961 as root reinforcement degraded (Harris and Farr, 1974; Wu et al., 1979). Wu et al. (1979) found that root strength about four years after clear-cutting was roughly 1/6 of virgin forest values, so we scaled our adopted root cohesion of 4.9 kPa accordingly and used 0.8 kPa to represent post-harvest conditions across the entire Maybeso region. Reduced root cohesion produced more widespread initiation and inundation that better captured the inventoried landslides, but also predicted debris flows on slopes without mapped landslides (Fig. S5). This indicates the model may be used to capture post-harvest instability, but the spatial extent of timber harvest should be explicitly defined to limit false positives in surrounding old-growth forests.

Similarity indices quantifying how well modeled landslides matched the inventory varied substantially between watersheds. Most similarity indices were negative, indicating imperfect spatial agreement. However, these values should be interpreted in the context of the scale of calibration, uncertainty in the heterogeneity of parameters, and the spatial imprecision of TNFLI landslide locations (commonly >10 m; Patton et al., 2022). Small differences in the mapped location of landslide initiation can produce substantial differences in modeled versus inventoried flow paths because a landslide initiated on one side of a drainage divide may be routed into a different downstream channel.

Similarity was also influenced by the amount of heterogeneity in debris-flow mobility within a given catchment. Similarity generally decreased as the coefficient of variation in H/L increased, indicating that watersheds containing debris flows with more heterogeneous mobility were more difficult to simulate with a single parameter set (Fig. S3). Thus, the spatial extent in which calibration occurs will determine how many debris flows are represented by a single parameter set. At the broadest scale, an entire landscape could be modeled by a single parameter set, but this assumes debris-flow characteristics are relatively homogenous and may produce poor agreement where characteristics differ from the majority of debris flows. Conversely, calibration at the hillslope scale could better capture localized variability, but this would substantially increase the number of parameter sets for forward modeling and would inhibit parameterization in locations where no debris flows have been historically observed.

Watershed-scale calibration is one intermediate solution that uses a manageable number of parameter sets to characterize variability in debris-flow mobility throughout a broad landscape. However, larger calibration units could be used depending on the size of the landscape or availability of inventories, highlighting an important modeling decision that must be considered on a case-to-case basis. Alternative approaches could define calibration units according to geology, soil series, or geomorphic or topographic characteristics, but this also presents challenges because individual debris flows commonly traverse multiple

https://doi.org/10.5194/egusphere-2026-6672
Preprint. Discussion started: 25 November 2026
© Author(s) 2026. CC BY 4.0 License.

environmental or geomorphic settings. Thus, selecting an appropriate calibration scale presents a trade-off between having sufficient observations to constrain model parameters and maintaining a sufficiently small area that captures landscape-scale variations in debris-flow characteristics.

5.3 Potential role of soil production and flux in debris-flow runout modeling

Although the calibration framework here uses empirical runout parameters, our results suggest that landscape evolution models may present a process-based means of constraining volumetric growth. In Grfin Tools and similar approaches, debris-flow volume increases at a constant prescribed rate within areas identified as growth zones. Therefore, these approaches assume that material is available for entrainment wherever the model permits growth. However, sediment availability is a prerequisite for entrainment, and the amount and spatial distribution of mobile sediment can vary throughout a landscape. Landscape evolution models based on widely available, high-resolution topographic data can explicitly model this variability by predicting the distribution and depth of colluvium from topography, soil production, and sediment flux.

This distinction is important because while debris flows typically travel through convergent, channelized areas with high curvature, the relationship between topographic convergence and colluvium depth is not necessarily monotonic (Figure 3). Convergent terrain with concave curvature commonly accumulates colluvium through sediment flux, and empirical relationships have consequently been developed to relate topographic curvature to colluvium depth (e.g., Catani et al., 2010). However, our results show that in some steep convergent areas, sediment flux can exceed soil production resulting in little to no colluvium thickness despite high curvature (Figure 3b; Figure 4).

This has direct implications for regional-scale debris-flow runout modeling. Grfin Tools and other entrainment-based approaches can define growth zones using stream slope, curvature, source-area ratio, stream order, or drainage area (Reid et al., 2025). These criteria provide proxies for identifying where entrainment is likely to occur, but they do not constrain the quantity of sediment available for entrainment. Therefore, applying an empirical volumetric growth factor in a steep channel where no colluvium is present may permit bulking where the empirical bulking rate exceeds the actual sediment supply, potentially overestimating debris-flow volume, and ultimately, inundation area. A modeled distribution of colluvium has the potential to inform a sediment-driven entrainment model, in which volumetric growth is determined by both topographic thresholds (e.g., channel slope) and the amount of erodible material available along the flow path.

To explore this concept, we compared the cumulative volume of upslope colluvium available for entrainment along a representative debris-flow path with the cumulative debris flow volume predicted using Grfin Tools (Figure **11**). The Grfin Tools simulation used the calibrated transition slope and volumetric growth factor for this watershed, whereas the colluvium-based calculation estimated the volume of material available upslope of the flow path within terrain exceeding the transition-slope threshold. Despite their different approaches, the two methods produced comparable rates of volumetric growth and total volumes along the modeled flow path. Although demonstrated for a single representative debris flow, this agreement highlights the potential for modeled sediment availability to provide a physical constraint on empirical bulking rates where direct measurements of entrainment are unavailable.

https://doi.org/10.5194/egusphere-2026-6672
Preprint. Discussion started: 25 November 2026
© Author(s) 2026. CC BY 4.0 License.

This approach could also reduce parameter uncertainty in regional-scale runout modeling while capturing heterogeneity in debris flow processes more directly. In the calibration framework presented here, both the transition slope and volumetric growth factor are optimized to maximize model performance, which can potentially be achieved using multiple, non-unique parameter combinations. If volumetric bulking were instead constrained using a spatial distribution of colluvium, transition slope or other parameters governing entrainment could be interpreted more directly, potentially providing additional insight into the physical controls governing debris-flow mobility, entrainment, and inundation throughout the landscape. This advance would also serve as a means of capturing the heterogeneity of debris flows, as it relates to sediment availability, more directly than an iterative optimization scheme based on a constant growth factor.

Additionally, such a framework could ultimately establish a basis for investigating temporal changes in debris flow magnitude and frequency. Debris-flow events evacuate stored hillslope and channel sediment, after which sediment is progressively replenished through hillslope transport and colluvial infilling. Models that explicitly capture sediment storage and transport could therefore provide a mechanism for investigating how the availability of sediment influences debris-flow size and recurrence through time (Jakob et al., 2005; Parker et al., 2016).

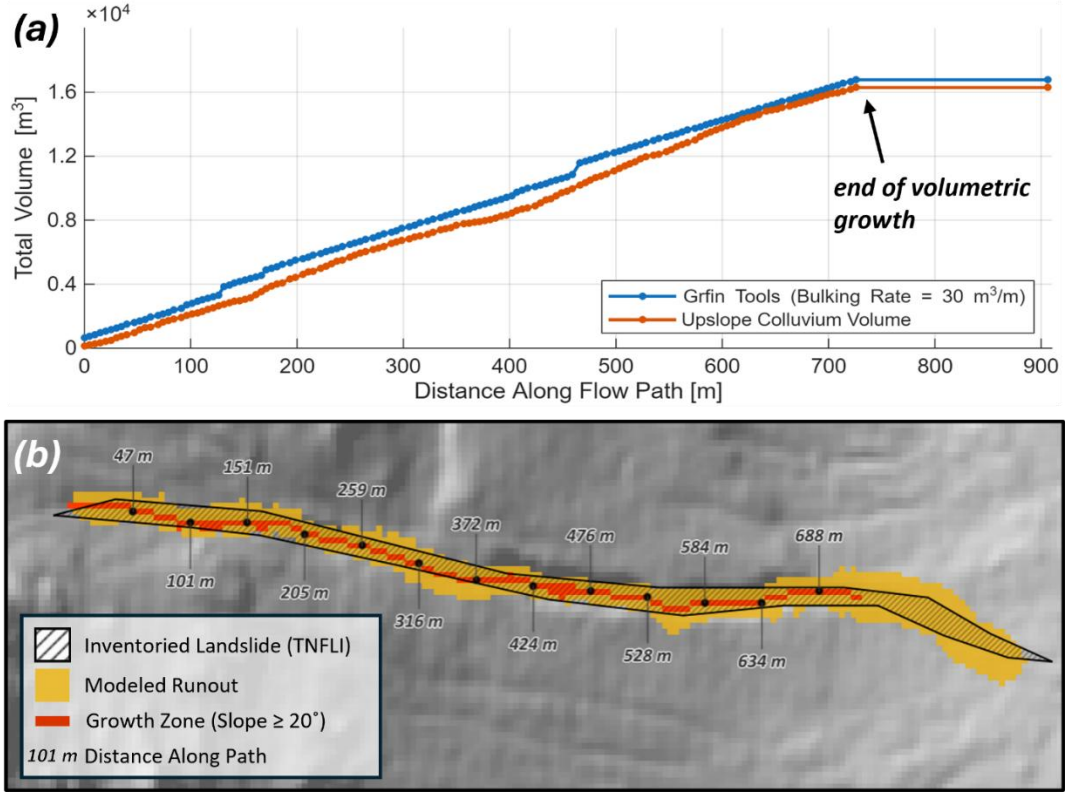

Figure 11 (a) Comparison of total volume vs. distance along flow path. The Grfin Tools volume (blue line) shows volumetric growth within the growth zone as defined by a constant bulking factor (30 m^3/m). The upslope colluvium volume (orange line) shows the summation of volume of all upslope soil columns where the terrain (within the inventoried landslide boundary) is steeper than the threshold for growth (20°). (b) Image of debris flow and growth zone with markers corresponding to "distance along flow path" in Figure 11a. Hillshade derived from lidar (Quantum Spatial, 2018, 2020).

https://doi.org/10.5194/egusphere-2026-6672
Preprint. Discussion started: 25 November 2026
© Author(s) 2026. CC BY 4.0 License.

5.4 Implications for landslide hazard and risk in Southeast Alaska

Regional-scale landslide susceptibility assessments commonly identify broad areas of unstable terrain but, in turn, often do not explicitly account for variations in colluvium thickness and groundwater redistribution at scales finer than the hillslope. In Southeast Alaska, where steep and high-relief terrain is widespread, these approaches can identify large portions of the landscape susceptible to landslides but are limited in their ability to distinguish unstable terrain features from surrounding stable terrain at scales relevant to communities and infrastructure. By incorporating finer-scale topographic controls on slope stability, our framework attains greater spatial specificity for assessing potential landslide initiation and downstream impacts at the community scale.

Resolving these finer-scale processes relies on the availability of high-resolution topographic data. Lidar provides the resolution required to identify hollows, ridges, channels, and other geomorphic features that govern colluvium accumulation and groundwater convergence, making it a vital data resource for regional assessments in Southeast Alaska and similar soil-mantled landscapes prone to landslides. However, lidar coverage remains incomplete in Southeast Alaska, especially multitemporal lidar which enables evaluation of landscape change associated to landsliding (Burns et al., 2025; Roering et al., 2025; Scheip and Wegmann, 2022). Multitemporal datasets can document changes associated with debris-flow erosion, transport, and deposition across a large sample of failures within a landscape, providing valuable observations for understanding regional debris-flow behavior and, ultimately, parameterizing runout models. Because these process-scale controls are difficult to capture using coarser topographic data, expanding high-resolution lidar coverage would directly increase the geographic extent over which this type of assessment can be applied.

Although identifying initiation potential is important for highlighting where landslides may begin, initiation susceptibility alone does not capture the full extent of potential debris-flow impacts. Rather, a complete characterization of susceptibility requires consideration of debris-flow inundation below initiation sites. By coupling initiation and inundation modeling, the resulting framework identifies not only where landslides are likely to begin, but also where debris flows may impact downslope communities and infrastructure. This is particularly important in Southeast Alaska, where communities are commonly situated on narrow coastal lowlands bounded by steep terrain, and transportation networks often consist of a limited number of roads connecting residents to critical services.

The intended outcomes of this modeling framework emerged through community engagement during the development of this study. Discussions with community and Tribal partners on Prince of Wales Island have highlighted the urgency of developing tools to anticipate disruptions to roads, infrastructure, fish-bearing streams, and communities from debris flows. Maps identifying inundation potential can help translate regional landslide processes into actionable spatial information supporting community planning and geohazard resilience.

https://doi.org/10.5194/egusphere-2026-6672
Preprint. Discussion started: 25 November 2026
© Author(s) 2026. CC BY 4.0 License.

5.5 Opportunities for improving regional-scale debris flow modeling

The framework presented here relies on simplified parameterizations of soil properties, hydrology, and debris-flow behavior to effectively model regional-scale landslide initiation and debris-flow inundation. These simplifications were necessary to apply the framework across a large and data-sparse landscape but also identify several opportunities to improve the physical characterization of landslide and debris-flow processes in landscapes like Southeast Alaska.

In this work, we rely on an empirical relationship derived from a sub-alpine catchment in Switzerland to relate geomorphic characteristics to hydrostatic pore pressure. This approach reflects the expected trend that convergent terrain is wetter than divergent terrain and generates a spatially distributed model of groundwater conditions using readily available topographic data. However, subsurface flow in Southeast Alaska is likely not captured by topography alone. Rather, the transmission of subsurface water is influenced by discontinuous and heterogeneous till deposits, fractured bedrock, and macropore flow (Patric and Swanston, 1968). Substantial uncertainty remains around how rainfall is translated into transient pore-pressure responses in the well-drained, high-saturation environment of Southeast Alaska (Mirus et al., 2024). Incorporating observations of subsurface hydrology and the transient pore-pressure response to rainfall could improve estimates of the conditions that promote landslide initiation and create a pathway toward evaluating landslide hazard in relation to storm recurrence.

Our results indicate that the landscape evolution model produced a spatial pattern of colluvium thickness consistent with those observed in soil-mantled landscapes. However, Southeast Alaska is a dynamic landscape in a relatively early stage of post-glacial development with variable extent of incision and slope modification. It remains an open question whether landscape evolution models developed for unglaciated landscapes account for the processes governing soil production, transport, and storage in Southeast Alaska. This does not preclude the use of landscape evolution models in the region but highlights an opportunity to evaluate how well process-based formulations simulate colluvial dynamics in post-glacial landscapes. Further, observations of colluvium thickness and hillslope sediment transport could be used to calibrate and evaluate these models and improve estimates of spatially variable colluvium depth in Southeast Alaska.

There are also opportunities to improve the coupling of initiation and runout modeling within a unified framework. Grfin Tools is an efficient means of simulating debris-flow inundation across large landscapes. However, its current implementation treats growth zones as additional initiation locations rather than requiring debris flows to originate only at explicitly defined initiation points. As a result, the model can generate debris flows in locations where the initiation model does not predict instability, producing unintended debris-flow artifacts inconsistent with modeled slope stability. A more physically connected approach would explicitly link initiation and runout such that inundation simulations originate only from unstable sites identified by the initiation model.

Finally, continued improvements of landslide inventories provide an opportunity to improve the utility of our calibration framework, which is based on similarity between modeled and inventoried landslides. This framework offers a practical approach for parameterizing debris-flow heterogeneity across landscapes, but uncertainty in the spatial positioning of inventoried landslides can strongly influence estimates of spatial agreement. In particular, small differences in initiation

https://doi.org/10.5194/egusphere-2026-6672
Preprint. Discussion started: 25 November 2026
© Author(s) 2026. CC BY 4.0 License.

location can route modeled debris flows into adjacent channels, resulting in substantial differences in spatial similarity. Improvements in landslide mapping precision and corrections to previously mapped landslides would improve regional-scale calibration using the approach presented here and could ultimately account for runout heterogeneity more accurately across large landscapes.

6 Conclusion

In this study, we coupled a physics-based landslide initiation model with a regional-scale debris-flow runout to estimate debris-flow inundation for a large swath of Prince of Wales Island, Alaska. We also computed the spatial distribution of colluvium depth using a landscape evolution model and estimated groundwater conditions from topographic wetness. By incorporating these spatially variable processes into the slope stability model, we were able to distinguish convergent, potentially unstable terrain from relatively stable, yet steep, adjacent terrain, resulting in strong discrimination between inventoried landslide initiation points and non-landslide locations (AUC = 0.86). Further, we assessed the interdependence of colluvium depth and soil saturation on slope stability and showed that colluvium availability sets the stage for failure by providing the prerequisite material for failure while groundwater acts as the trigger to initiate shallow landslides. Importantly, both conditions must coincide for landslide initiation to occur.

We also showed that regional-scale debris-flow inundation can be modeled in data-sparse environments using local calibration of empirical runout parameters. We optimized the volumetric bulking rate and slope threshold for entrainment by comparing the spatial similarity of modeled and inventoried debris flows and performed this calibration independently within each HUC-14 watershed to account for heterogeneity in debris-flow mobility throughout a large landscape. Our results also demonstrated the potential to extend the role of modeled colluvium depth to parameterizing the runout model. Because the landscape evolution model predicts where sediment is stored throughout the landscape, its spatial distribution could provide a constraint on how much material is available for entrainment and help parameterize runout models where direct measurements of sediment supply are unavailable.

By characterizing instability at scales finer than that of hillslopes, our approach differs from many regional-scale susceptibility models that use first-order topographic metrics to identify large regions of potentially unstable terrain, resulting in high rates of false positives. Further, our coupled debris-flow initiation and inundation framework captures inundation areas where landslide impacts may extend substantially further downstream than the initiation area. Together, these components generate maps of debris-flow susceptibility at scales relevant to individual communities that can help characterize potential exposure of roads, infrastructure, and communities to debris flows. The objectives of this work were determined through iterative engagement with Tribal governments and community members on Prince of Wales Island. More broadly, the framework demonstrates how high-resolution topography, process-based hillslope modeling, and empirically calibrated runout modeling can be combined to assess debris-flow susceptibility across large, data-sparse landscapes.

https://doi.org/10.5194/egusphere-2026-6672
Preprint. Discussion started: 25 November 2026
© Author(s) 2026. CC BY 4.0 License.

Code and data availability

The MATLAB code used to model landslide initiation, calculate AUC and ROC curves, process inputs for Grfin Tools, and calibrate runout parameters, along with model input rasters and supplementary maps, are available at https://doi.org/10.5281/zenodo.23681876 (Mathews and Roering, 2026). Any updates or maintenance to the code will be hosted at https://github.com/Sitka-Sound-Science-Center/debris-flow-initiation-runout. Grfin Tools version 1.0 is available at https://doi.org/10.5066/P9NVKFE2 (Cronkite-Ratcliff et al., 2025). Lidar-derived elevation data were obtained from the Alaska Division of Geological & Geophysical Surveys Elevation Portal (https://elevation.alaska.gov; Quantum Spatial, 2018, 2020). The Tongass National Forest Landslide Inventory is available from https://catalog.data.gov/dataset/tongass-landslide-areas-feature-layer (U.S. Forest Service, 2024a, b). Soil series data were obtained from https://akgeoportal.alaska.gov/maps/f5c457ee784d4ccc871f8c2d8cb02780/about (U.S. Forest Service, 2020). Watershed boundaries were obtained from https://www.sciencebase.gov/catalog/item/6930876ed4be027594fed169 (U.S. Geological Survey, 2026). Groundwater and topographic wetness index data used to develop the saturation relationship were digitized from Rinderer et al. (2014).

Supplement link

The supplement is available online.

Author contributions

NWM contributed to research conceptualization, data curation, analysis, design of methodology, software development, validation, visualization, and original draft preparation. JJR contributed to research conceptualization, funding acquisition, design of methodology, supervision, and original draft preparation. ACJ contributed to research conceptualization. LS contributed to research conceptualization, project administration, and supervision. SM contributed to research conceptualization and data curation. LB contributed to project administration and supervision. All authors reviewed and edited the manuscript.

Competing interests

The authors declare that they have no competing interests.

https://doi.org/10.5194/egusphere-2026-6672
Preprint. Discussion started: 25 November 2026
© Author(s) 2026. CC BY 4.0 License.

Disclaimer

Copernicus Publications remains neutral with regard to jurisdictional claims made in the text, published maps, institutional affiliations, or any other geographical representation in this paper. While Copernicus Publications makes every effort to include appropriate place names, the final responsibility lies with the authors. Views expressed in the text are those of the authors and do not necessarily reflect the views of the publisher.

Acknowledgements

We thank the Klawock Cooperative Association (KCA), Craig Tribal Association (CTA), and Organized Village of Kasaan (OVK) for their partnership in this work and for steering the development and application of the study. We thank Quinn Aboudara, a Prince of Wales Island resident, for sharing local observations that informed our understanding of landslide processes. We thank Dianne Brien and Mark Reid for their support with implementation of Grfin Tools. We also thank Ries Plescher, Deanna Nash, Andrea Vale, and the Alaska Youth Stewards for assistance with fieldwork on Prince of Wales Island, and KK Prussian (U.S. Forest Service, Sitka Ranger District) for facilitating field visits and sharing expertise on landslides in Southeast Alaska. Claude (Anthropic) was used to assist with writing and debugging the ROC/AUC validation code. All code was reviewed and verified by the lead author.

Financial support

This work was supported by the National Science Foundation (NSF) Coastlines and People (CoPE) program through the Kutí Project (Award No. 2052972) and Alaska Sea Grant (Award No. NA24OARX417C0229-T1-01).

References

Alaska Division of Geological & Geophysical Surveys: Alaska Elevation Portal, https://elevation.alaska.gov/ (last access: 16 October 2026), 2026.

Alberti, S., Leshchinsky, B., Roering, J., Perkins, J., and Olsen, M. J.: Inversions of landslide strength as a proxy for subsurface weathering, Nat Commun, 13, 6049, https://doi.org/10.1038/s41467-022-33798-5, 2022.

https://doi.org/10.5194/egusphere-2026-6672
Preprint. Discussion started: 25 November 2026
© Author(s) 2026. CC BY 4.0 License.

Alvioli, M., Guzzetti, F., and Rossi, M.: Scaling properties of rainfall induced landslides predicted by a physically based model, Geomorphology, 213, 38–47, https://doi.org/10.1016/j.geomorph.2013.12.039, 2014.

Baichtal, J. F., Lesnek, A. J., Carlson, R. J., Schmuck, N. S., Smith, J. L., Landwehr, D. J., and Briner, J. P.: Late Pleistocene and early Holocene sea-level history and glacial retreat interpreted from shell-bearing marine deposits of southeastern Alaska, USA, Geosphere, 17, 1590–1615, https://doi.org/10.1130/GES02359.1, 2021.

Baum, R. L., Savage, W. Z., and Godt, J. W.: TRIGRS: a Fortran program for transient rainfall infiltration and grid-based regional slope-stability analysis, version 2.0, US Geological Survey, Reston, VA, USA, 2008.

Baum, R. L., Godt, J. W., and Savage, W. Z.: Estimating the timing and location of shallow rainfall-induced landslides using a model for transient, unsaturated infiltration, J. Geophys. Res., 115, F03013, https://doi.org/10.1029/2009JF001321, 2010.

Bellugi, D., Milledge, D. G., Dietrich, W. E., McKean, J. A., Perron, J. T., Sudderth, E. B., and Kazian, B.: A spectral clustering search algorithm for predicting shallow landslide size and location: A shallow landslide search algorithm, J. Geophys. Res. Earth Surf., 120, 300–324, https://doi.org/10.1002/2014JF003137, 2015.

Berger, C., McArdell, B. W., and Schlunegger, F.: Direct measurement of channel erosion by debris flows, Illgraben, Switzerland: DEBRIS FLOW EROSION, J. Geophys. Res., 116, n/a-n/a, https://doi.org/10.1029/2010JF001722, 2011.

Berti, M. and Simoni, A.: Prediction of debris flow inundation areas using empirical mobility relationships, Geomorphology, 90, 144–161, https://doi.org/10.1016/j.geomorph.2007.01.014, 2007.

Beven, K. J. and Kirkby, M. J.: A physically based, variable contributing area model of basin hydrology / Un modèle à base physique de zone d'appel variable de l'hydrologie du bassin versant, Hydrological Sciences Bulletin, 24, 43–69, https://doi.org/10.1080/02626667909491834, 1979.

Bishop, D. M. and Stevens, M. E.: Landslides on logged areas in southeast Alaska, Northern Forest Experiment Station, Forest Service, US Department of Agriculture, 1964.

Booth, A. M., Sifford, C., Vascik, B., Siebert, C., and Buma, B.: Large wood inhibits debris flow runout in forested southeast Alaska, Earth Surf Processes Landf, 45, 1555–1568, https://doi.org/10.1002/esp.4830, 2020.

Brien, D. L., Reid, M. E., Cronkite-Ratcliff, C., and Perkins, J. P.: Topographic controls on landslide mobility: modeling hurricane-induced landslide runout and debris-flow inundation in Puerto Rico, Nat. Hazards Earth Syst. Sci., 25, 1229–1253, https://doi.org/10.5194/nhess-25-1229-2025, 2025.

British Oceanographic Data Centre: Polygon dataset of the extent of water bodies from the SeaVoX Salt and Fresh Water Body Gazetteer (v19), https://doi.org/10.14284/590, 2023.

Buma, B. and Johnson, A. C.: The role of windstorm exposure and yellow cedar decline on landslide susceptibility in southeast Alaskan temperate rainforests, Geomorphology, 228, 504–511, https://doi.org/10.1016/j.geomorph.2014.10.014, 2015.

Bunn, M., Leshchinsky, B., and Olsen, M. J.: Estimates of three-dimensional rupture surface geometry of deep-seated landslides using landslide inventories and high-resolution topographic data, Geomorphology, 367, 107332, https://doi.org/10.1016/j.geomorph.2020.107332, 2020a.

Bunn, M., Leshchinsky, B., and Olsen, M. J.: Geologic Trends in Shear Strength Properties Inferred Through Three-Dimensional Back Analysis of Landslide Inventories, J. Geophys. Res. Earth Surf., 125, https://doi.org/10.1029/2019JF005461, 2020b.

https://doi.org/10.5194/egusphere-2026-6672
Preprint. Discussion started: 25 November 2026
© Author(s) 2026. CC BY 4.0 License.

Burns, W. J., Calhoun, N. C., and Franczyk, J. J.: Protocol for Channelized Debris Flow Susceptibility Mapping (Special Paper 53), Oregon Department of Geology and Mineral Industries, 2022.

Burns, W. J., Calhoun, N. C., Zimmerman, M., Roering, J. J., Sanders, M. A., Leshchinsky, B. A., Sousa, F. D. M. D., Olsen, M. J., Rengers, F. K., and Mathews, N. W.: Multitemporal LiDAR analysis of pre- and post-Eagle Creek Fire debris flows, western Columbia River Gorge, Hood River and Multnomah Counties, Oregon, Special Paper 55, Oregon Department of Geology and Mineral Industries, Portland, Oregon, 2025.

Carrara, P. E., Ager, T. A., Baichtal, J. F., and VanSistine, D. P.: Map of glacial limits and possible refugia in the southern Alexander Archipelago, Alaska, during the late Wisconsin glaciation, https://doi.org/10.3133/mf2424, 2003.

Catani, F., Segoni, S., and Falorni, G.: An empirical geomorphology-based approach to the spatial prediction of soil thickness at catchment scale, Water Resources Research, 46, 2008WR007450, https://doi.org/10.1029/2008WR007450, 2010.

Christen, M., Kowalski, J., and Bartelt, P.: RAMMS: Numerical simulation of dense snow avalanches in three-dimensional terrain, Cold Regions Science and Technology, 63, 1–14, https://doi.org/10.1016/j.coldregions.2010.04.005, 2010.

Corominas, J., Van Westen, C., Frattini, P., Cascini, L., Malet, J.-P., Fotopoulou, S., Catani, F., Van Den Eeckhaut, M., Mavrouli, O., Agliardi, F., Pitilakis, K., Winter, M. G., Pastor, M., Ferlisi, S., Tofani, V., Hervás, J., and Smith, J. T.: Recommendations for the quantitative analysis of landslide risk, Bull Eng Geol Environ, https://doi.org/10.1007/s10064-013-0538-8, 2013.

Cronkite-Ratcliff, C., Reid, M. E., Brien, D. L., and Perkins, J. P.: Grfin Tools—Software Package and Runtime Documentation for Users, https://doi.org/10.5066/P9NVKFE2, 2025.

Darrow, M. M. and Jacobs, A.: Read all about it! A review of more than a century of Alaskan landslides as recorded in periodicals, Landslides, 23, 807–821, https://doi.org/10.1007/s10346-025-02663-z, 2026.

Darrow, M. M., Nelson, V. A., Grilliot, M., Wartman, J., Jacobs, A., Baichtal, J. F., and Buxton, C.: Geomorphology and initiation mechanisms of the 2020 Haines, Alaska landslide, Landslides, 19, 2177–2188, https://doi.org/10.1007/s10346-022-01899-3, 2022.

Dietrich, W. E., Reiss, R., Hsu, M.-L., and Montgomery, D. R.: A process-based model for colluvial soil depth and shallow landsliding using digital elevation data, Hydrological Processes, 9, 383–400, https://doi.org/https://doi.org/10.1002/hyp.3360090311, 1995.

Dietrich, W. E., Wilson, C. J., and Reneau, S. L.: Hollows, colluvium, and landslides in soil-mantled landscapes, in: Hillslope Processes, edited by: Abrahams, A. D., Routledge, 362–388, https://doi.org/10.4324/9781003028840-17, 2020.

Filz, G.: Engineering properties of Southeast Alaskan forest soils, 1981.

Geertsema, M. and Pojar, J. J.: Influence of landslides on biophysical diversity — A perspective from British Columbia, Geomorphology, 89, 55–69, https://doi.org/10.1016/j.geomorph.2006.07.019, 2007.

Gehrels, G. E.: Late Proterozoic-Cambrian metamorphic basement of the Alexander terrane on Long and Dall Islands, southeast Alaska, Geological Society of America Bulletin, 102, 760–767, https://doi.org/10.1130/0016-7606(1990)102%3C0760:LPCMBO%3E2.3.CO;2, 1990.

Godt, J. W., Baum, R. L., and Chleborad, A. F.: Rainfall characteristics for shallow landsliding in Seattle, Washington, USA, Earth Surf. Process. Landforms, 31, 97–110, https://doi.org/10.1002/esp.1237, 2006.

https://doi.org/10.5194/egusphere-2026-6672
Preprint. Discussion started: 25 November 2026
© Author(s) 2026. CC BY 4.0 License.

Gomi, T., Sidle, R. C., and Swanston, D. N.: Hydrogeomorphic linkages of sediment transport in headwater streams, Maybeso Experimental Forest, southeast Alaska, Hydrological Processes, 18, 667–683, https://doi.org/10.1002/hyp.1366, 2004.

Gong, W., Zekkos, D., and Clark, M.: A pseudo-3D methodology for regional-scale back-analysis of earthquake-induced landslides, Engineering Geology, 325, 107277, https://doi.org/10.1016/j.enggeo.2023.107277, 2023.

Gorr, A. N., McGuire, L. A., Youberg, A. M., and Rengers, F. K.: A progressive flow-routing model for rapid assessment of debris-flow inundation, Landslides, 19, 2055–2073, https://doi.org/10.1007/s10346-022-01890-y, 2022.

Griswold, J. and Iverson, R.: Mobility statistics and automated hazard mapping for debris flows and rock avalanches, Scientific Investigations Report, 2007–5276, Reston, VA, https://doi.org/10.3133/sir20075276, 2008.

Guzzetti, F., Ardizzone, F., Cardinali, M., Rossi, M., and Valigi, D.: Landslide volumes and landslide mobilization rates in Umbria, central Italy, Earth and Planetary Science Letters, 279, 222–229, https://doi.org/10.1016/j.epsl.2009.01.005, 2009.

Harris, A. S. and Farr, W. A.: The forest ecosystem of southeast Alaska: forest ecology and timber management, Pacific Northwest Research Station, US Department of Agriculture, Forest Service, 1974.

Heimsath, A. M., E. Dietrich, W., Nishiizumi, K., and Finkel, R. C.: Cosmogenic nuclides, topography, and the spatial variation of soil depth, Geomorphology, 27, 151–172, https://doi.org/10.1016/S0169-555X(98)00095-6, 1999.

Heimsath, A. M., DiBiase, R. A., and Whipple, K. X.: Soil production limits and the transition to bedrock-dominated landscapes, Nature Geosci, 5, 210–214, https://doi.org/10.1038/ngeo1380, 2012.

Heiser, M., Scheidl, C., and Kaitna, R.: Evaluation concepts to compare observed and simulated deposition areas of mass movements, Comput Geosci, 21, 335–343, https://doi.org/10.1007/s10596-016-9609-9, 2017.

Highland, L. and Bobrowsky, P. T.: The landslide handbook: a guide to understanding landslides, US Geological Survey Reston, 2008.

Horton, P., Jaboyedoff, M., Rudaz, B., and Zimmermann, M.: Flow-R, a model for susceptibility mapping of debris flows and other gravitational hazards at a regional scale, Nat. Hazards Earth Syst. Sci., 13, 869–885, https://doi.org/10.5194/nhess-13-869-2013, 2013.

Hosmer, D. W., Lemeshow, S., and Sturdivant, R. X.: Applied logistic regression, Third edition., Wiley, Hoboken, New Jersey, 500 pp., 2013.

Hungr, O.: A model for the runout analysis of rapid flow slides, debris flows, and avalanches, Can. Geotech. J., 32, 610–623, https://doi.org/10.1139/t95-063, 1995.

Hungr, O., Leroueil, S., and Picarelli, L.: The Varnes classification of landslide types, an update, Landslides, 11, 167–194, https://doi.org/10.1007/s10346-013-0436-y, 2014.

Iverson, R. M.: The physics of debris flows, Rev. Geophys., 35, 245–296, https://doi.org/10.1029/97RG00426, 1997.

Iverson, R. M.: Landslide triggering by rain infiltration, Water Resour. Res., 36, 1897–1910, https://doi.org/10.1029/2000WR900090, 2000.

https://doi.org/10.5194/egusphere-2026-6672
Preprint. Discussion started: 25 November 2026
© Author(s) 2026. CC BY 4.0 License.

Iverson, R. M. and George, D. L.: A depth-averaged debris-flow model that includes the effects of evolving dilatancy. I. Physical basis, Proceedings of the Royal Society A: Mathematical, Physical and Engineering Sciences, 470, 20130819, https://doi.org/10.1098/rspa.2013.0819, 2014.

Iverson, R. M., Schilling, S. P., and Vallance, J. W.: Objective delineation of lahar-inundation hazard zones, Geological Society of America Bulletin, 110, 972–984, https://doi.org/10.1130/0016-7606(1998)110%3C0972:ODOLIH%3E2.3.CO;2, 1998.

Jakob, M., Bovis, M., and Oden, M.: The significance of channel recharge rates for estimating debris-flow magnitude and frequency, Earth Surf Processes Landf, 30, 755–766, https://doi.org/10.1002/esp.1188, 2005.

Johnson, A. C. and Wilcock, P.: Association between cedar decline and hillslope stability in mountainous regions of southeast Alaska, Geomorphology, 46, 129–142, https://doi.org/10.1016/S0169-555X(02)00059-4, 2002.

Johnson, A. C., Swanston, D. N., and McGee, K. E.: LANDSLIDE INITIATION, RUNOUT, AND DEPOSITION WITHIN CLEARCUTS AND OLD-GROWTH FORESTS OF ALASKA[1], J American Water Resour Assoc, 36, 17–30, https://doi.org/10.1111/j.1752-1688.2000.tb04245.x, 2000.

Kassem, M. and Zekkos, D.: Assessing rainfall-induced landslide failure mechanisms in regional hydrological and hillslope stability simulations, Landslides, 23, 933–952, https://doi.org/10.1007/s10346-025-02690-w, 2026.

Keck, J., Istanbulluoglu, E., Campforts, B., Tucker, G., and Horner-Devine, A.: A landslide runout model for sediment transport, landscape evolution, and hazard assessment applications, Earth Surf. Dynam., 12, 1165–1191, https://doi.org/10.5194/esurf-12-1165-2024, 2024.

Kheiry, L.: Big landslide blocks South Thorne Bay/Kasaan Road, 2019.

Lawrence, E., Luna, L., Patton, A., Mirus, B., Jacobs, A., and Roering, J.: News-reported landslide impacts in Southeast Alaska, 1990-2024, https://doi.org/10.5066/P1EOCB5J, 2025.

Lu, N. and Likos, W. J.: Suction Stress Characteristic Curve for Unsaturated Soil, J. Geotech. Geoenviron. Eng., 132, 131–142, https://doi.org/10.1061/(ASCE)1090-0241(2006)132:2(131), 2006.

Lu, N. and Likos, W. J.: Origin of Cohesion and Its Dependence on Saturation for Granular Media, in: Poromechanics V, Fifth Biot Conference on Poromechanics, 1669–1675, https://doi.org/10.1061/9780784412992.197, 2013.

Martin, Y., Rood, K., Schwab, J. W., and Church, M.: Sediment transfer by shallow landsliding in the Queen Charlotte Islands, British Columbia, Can. J. Earth Sci., 39, 189–205, https://doi.org/10.1139/e01-068, 2002.

Mathews, N. W. and Roering, J. J.: Code, data, and susceptibility maps for coupled landslide initiation and debris-flow runout modeling, Prince of Wales Island, Alaska (1.0), https://doi.org/10.5281/zenodo.23681876, 2026.

Mathews, N. W., Leshchinsky, B. A., Mirus, B. B., Olsen, M. J., and Booth, A. M.: RegionGrow3D: A Deterministic Analysis for Characterizing Discrete Three-Dimensional Landslide Source Areas on a Regional Scale, Journal of Geophysical Research: Earth Surface, 129, e2024JF007815, https://doi.org/10.1029/2024JF007815, 2024.

McDougall, S.: 2014 Canadian Geotechnical Colloquium: Landslide runout analysis — current practice and challenges, Can. Geotech. J., 54, 605–620, https://doi.org/10.1139/cgj-2016-0104, 2017.

McDougall, S. and Hungr, O.: A model for the analysis of rapid landslide motion across three-dimensional terrain, Can. Geotech. J., 41, 1084–1097, https://doi.org/10.1139/t04-052, 2004.

https://doi.org/10.5194/egusphere-2026-6672
Preprint. Discussion started: 25 November 2026
© Author(s) 2026. CC BY 4.0 License.

Menounos, B., Goehring, B. M., Osborn, G., Margold, M., Ward, B., Bond, J., Clarke, G. K. C., Clague, J. J., Lakeman, T., Koch, J., Caffee, M. W., Gosse, J., Stroeven, A. P., Seguinot, J., and Heyman, J.: Cordilleran Ice Sheet mass loss preceded climate reversals near the Pleistocene Termination, Science, 358, 781–784, https://doi.org/10.1126/science.aan3001, 2017.

Milledge, D. G., Bellugi, D., McKean, J. A., Densmore, A. L., and Dietrich, W. E.: A multidimensional stability model for predicting shallow landslide size and shape across landscapes: predicting landslide size and shape, J. Geophys. Res. Earth Surf., 119, 2481–2504, https://doi.org/10.1002/2014JF003135, 2014.

Mirus, B. B., Belair, G. M., Wood, N. J., Jones, J., and Martinez, S. N.: Parsimonious High-Resolution Landslide Susceptibility Modeling at Continental Scales, AGU Advances, 5, e2024AV001214, https://doi.org/10.1029/2024AV001214, 2024.

Mirus, B. B., Bogaard, T., Greco, R., and Stähli, M.: Invited perspectives: Integrating hydrologic information into the next generation of landslide early warning systems, Nat. Hazards Earth Syst. Sci., 25, 169–182, https://doi.org/10.5194/nhess-25-169-2025, 2025.

Montgomery, D. R. and Dietrich, W. E.: A physically based model for the topographic control on shallow landsliding, Water Resources Research, 30, 1153–1171, https://doi.org/https://doi.org/10.1029/93WR02979, 1994.

Moon, S., Formetta, G., Higa, J. T., Busti, R., Bellugi, D. G., Milledge, D. G., Ebel, B. A., and Dietrich, W. E.: Deep critical zone controls on shallow landslides, Proc. Natl. Acad. Sci. U.S.A., 123, e2524542123, https://doi.org/10.1073/pnas.2524542123, 2026.

Moran, T.: Petersburg plans for landslides, , Alaska Sea Grant News, 2026.

Nash, D., Rutz, J. J., and Jacobs, A.: Atmospheric Rivers in Southeast Alaska: Meteorological Conditions Associated With Extreme Precipitation, JGR Atmospheres, 129, e2023JD039294, https://doi.org/10.1029/2023JD039294, 2024.

Nicolazzo, J. A. and Larsen, M. C.: Landslide hazard susceptibility mapping in Haines, Alaska, RI 2024-8, Alaska Division of Geological & Geophysical Surveys, https://doi.org/10.14509/31309, 2025.

Pack, R. T., Tarboton, D. G., and Goodwin, C. N.: The SINMAP approach to terrain stability mapping, 1998.

Palecki, M., Durre, I., Applequist, S., Arguez, A., and Lawrimore, J.: U.S. Climate Normals 2020: U.S. Annual/Seasonal Climate Normals (1991-2020), https://doi.org/10.25921/4ek7-fk11, 2021.

Parker, R. N., Hales, T. C., Mudd, S. M., Grieve, S. W. D., and Constantine, J. A.: Colluvium supply in humid regions limits the frequency of storm-triggered landslides, Sci Rep, 6, 34438, https://doi.org/10.1038/srep34438, 2016.

Patric, J. H. and Swanston, D. N.: Hydrology of A Slide-Prone Glacial Till Soil in Southeast Alaska, Journal of Forestry, 66, 62–66, https://doi.org/10.1093/jof/66.1.62, 1968.

Patton, A. I., Roering, J. J., and Orland, E.: Debris flow initiation in postglacial terrain: Insights from shallow landslide initiation models and geomorphic mapping in Southeast Alaska, Earth Surf Processes Landf, 47, 1583–1598, https://doi.org/10.1002/esp.5336, 2022.

Patton, A. I., Luna, L. V., Roering, J. J., Jacobs, A., Korup, O., and Mirus, B. B.: Landslide initiation thresholds in data-sparse regions: application to landslide early warning criteria in Sitka, Alaska, USA, Nat. Hazards Earth Syst. Sci., 23, 3261–3284, https://doi.org/10.5194/nhess-23-3261-2023, 2023.

https://doi.org/10.5194/egusphere-2026-6672
Preprint. Discussion started: 25 November 2026
© Author(s) 2026. CC BY 4.0 License.

Patton, N. R., Lohse, K. A., Godsey, S. E., Crosby, B. T., and Seyfried, M. S.: Predicting soil thickness on soil mantled hillslopes, Nat Commun, 9, 3329, https://doi.org/10.1038/s41467-018-05743-y, 2018.

Pollock, W. and Wartman, J.: Disaggregation of Landslide Risk, Earth's Future, 14, e2025EF007594, https://doi.org/10.1029/2025EF007594, 2026.

Prancevic, J. P., Lamb, M. P., McArdell, B. W., Rickli, C., and Kirchner, J. W.: Decreasing Landslide Erosion on Steeper Slopes in Soil-Mantled Landscapes, Geophysical Research Letters, 47, e2020GL087505, https://doi.org/10.1029/2020GL087505, 2020.

Quantum Spatial, Inc.: 2017 USGS Lidar: Prince of Wales Island, AK, https://www.fisheries.noaa.gov/inport/item/58254 (last access: 18 October 2026), 2018.

Quantum Spatial, Inc.: 2018 USGS Lidar: Prince of Wales Island - Phase 2, AK, https://www.fisheries.noaa.gov/inport/item/59311 (last access: 18 October 2026), 2020.

Quinn, P. F., Beven, K. J., and Lamb, R.: The in(a /tan/β) index: How to calculate it and how to use it within the topmodel framework, Hydrological Processes, 9, 161–182, https://doi.org/10.1002/hyp.3360090204, 1995.

Reichenbach, P., Rossi, M., Malamud, B. D., Mihir, M., and Guzzetti, F.: A review of statistically-based landslide susceptibility models, Earth-Science Reviews, 180, 60–91, https://doi.org/10.1016/j.earscirev.2018.03.001, 2018.

Reid, M., Brien, D., Cronkite-Ratcliff, C., and Perkins, J.: Grfin Tools—User guide and methods for modeling landslide runout and debris-flow growth and inundation, Techniques and Methods, 14-A3, Reston, VA, https://doi.org/10.3133/tm14A3, 2025.

Reid, M. E., Coe, J. A., and Brien, D. L.: Forecasting inundation from debris flows that grow volumetrically during travel, with application to the Oregon Coast Range, USA, Geomorphology, 273, 396–411, https://doi.org/10.1016/j.geomorph.2016.07.039, 2016.

Reid, M. E., Cerovski-Darriau, C., Brien, D. L., Leb, I. H., and Cyr, A. J.: From start to stop: Simple methods for mapping susceptibility to landslide runout and debris-flow inundation, Landslides, 23, 3157–3170, https://doi.org/10.1007/s10346-026-02751-8, 2026.

Rinderer, M., Van Meerveld, H. J., and Seibert, J.: Topographic controls on shallow groundwater levels in a steep, prealpine catchment: When are the TWI assumptions valid?, Water Resources Research, 50, 6067–6080, https://doi.org/10.1002/2013WR015009, 2014.

Roering, J. J.: How well can hillslope evolution models "explain" topography? Simulating soil transport and production with high-resolution topographic data, Geological Society of America Bulletin, 120, 1248–1262, https://doi.org/10.1130/B26283.1, 2008.

Roering, J. J., Darrow, M., Patton, A., and Jacobs, A.: Bedrock ledges, colluvial wedges, and ridgetop water towers: Characterizing geomorphic and atmospheric controls on the 2023 Wrangell landslide to inform landslide assessment in Southeast Alaska, USA, https://doi.org/10.5194/egusphere-2025-4123, 9 September 2025., 2025.

Roering, J. J., Lawrence, E. R., Plescher, R., Sanders, M. A., Nash, D., Patton, A. I., Johnson, A., Jacobs, A., Mathews, N. W., Salomon, L., McKay, S., Schwanghart, W., Struble, W., and Aboudara, Q.: Shallow Landslides Align With Atmospheric Rivers in Coastal Steeplands, Geophysical Research Letters, 53, e2026GL124294, https://doi.org/10.1029/2026GL124294, 2026.

https://doi.org/10.5194/egusphere-2026-6672
Preprint. Discussion started: 25 November 2026
© Author(s) 2026. CC BY 4.0 License.



Salisbury, J. B.: Landslide hazard susceptibility mapping in Homer, Alaska, RI 2024-3, Alaska Division of Geological & Geophysical Surveys, https://doi.org/10.14509/31155, 2024.

Scheip, C. and Wegmann, K.: Insights on the growth and mobility of debris flows from repeat high-resolution lidar, Landslides, 19, 1297–1319, https://doi.org/10.1007/s10346-022-01862-2, 2022.

Schroeder, W.: Geotechnical properties of southeast Alaskan forest soils, USDA Forest Service Report, Civ. Engr. Dept., Oregon State University, Corvallis, Ore., Dec, 1983.

Schroeder, W. L. and Swanston, D. N.: Application of Geotechnical Data to Resource Planning in Southeast Alaska, PNW-198, US Department of Agriculture, Forest Service, Pacific Northwest Research Station, 1987.

Schuster, R. L. and Highland, L. M.: Overview of the Effects of Mass Wasting on the Natural Environment, Environmental and Engineering Geoscience, 13, 25–44, https://doi.org/10.2113/gseegeosci.13.1.25, 2007.

Sidle, R. C.: Shallow groundwater fluctuations in unstable hillslopes of coastal Alaska, Zeitschrift fur Gletscherkunde und Glazialgeologie, 20, 79–95, 1984.

Sidle, R. C.: A Conceptual Model of Changes in Root Cohesion in Response to Vegetation Management, J. environ. qual., 20, 43–52, https://doi.org/10.2134/jeq1991.00472425002000010009x, 1991.

Swanston, D. N.: Mass wasting in coastal Alaska, USDA Forest Service Research Paper PNW-83, Institute of Northern Forestry, Juneau, Alaska, 1969.

Swanston, D. N.: Mechanics of debris avalanching in shallow till soils of southeast Alaska, Pacific Northwest Forest and Range Experiment Station, Institute of Northern Forestry, 1970.

Swanston, D. N. and Marion, D. A.: Landslide response to timber harvest in southeast Alaska, Proceedings of the Fifth Federal Interagency Sedimentation Conference, 10–49, 1991.

Taylor, D. W.: Fundamentals of Soil Mechanics, Soil Science, 66, 1948.

Terzaghi, K.: Mechanism of Landslides, in: Application of Geology to Engineering Practice, edited by: Paige, S., Geological Society of America, https://doi.org/10.1130/Berkey.1950.83, 1950.

U.S. Census Bureau: 2018 Cartographic Boundary File, Current State and Equivalent for United States, 1:5,000,000, https://www2.census.gov/geo/tiger/GENZ2018/shp/cb_2018_us_state_5m.zip (last access: 25 November 2026), 2019.

U.S. Forest Service: Tongass National Forest Soils, https://akgeoportal.alaska.gov/maps/f5c457ee784d4ccc871f8c2d8cb02780/about, 2020.

U.S. Forest Service: Tongass Landslide Areas, https://catalog.data.gov/dataset/tongass-landslide-areas-feature-layer, 2024a.

U.S. Forest Service: Tongass Landslide Initiation, https://catalog.data.gov/dataset/tongass-landslide-areas-feature-layer, 2024b.

U.S. Geological Survey: USGS 3D Hydrography Program (3DHP) Downloadable Datasets 2025, https://www.sciencebase.gov/catalog/item/6930876ed4be027594fed169, 2026.

https://doi.org/10.5194/egusphere-2026-6672
Preprint. Discussion started: 25 November 2026
© Author(s) 2026. CC BY 4.0 License.

USDA Forest Service: Draft geology and geologic hazards assessment, Tongass National Forest plan revision, USDA Forest Service, Alaska Region, Tongass National Forest, Alaska, USA, https://www.fs.usda.gov/sites/nfs/files/legacy-media/tongass/Draft%20Assessment%20Geology%20and%20Geologic%20Hazards.pdf, 2024.

Walker, L. R. and Shiels, A. B.: Landslide ecology, Cambridge University Press, 2012.

Wu, T. H., McKinnell III, W. P., and Swanston, D. N.: Strength of tree roots and landslides on Prince of Wales Island, Alaska, Can. Geotech. J., 16, 19–33, https://doi.org/10.1139/t79-003, 1979.